




# Tower Models for Power Systems Transients: A Review

Erika Stracqualursi <sup>1,†</sup>, Giuseppe Pelliccione <sup>2,†</sup>, Salvatore Celozzi <sup>1,\*</sup> and Rodolfo Araneo <sup>1,†</sup>

<sup>1</sup> DIAEE—Electrical Engineering Division, University of Rome “La Sapienza”, Via Eudossiana 18, 00184 Rome, Italy; erika.stracqualursi@uniroma1.it (E.S.); rodolfo.araneo@uniroma1.it (R.A.)

<sup>2</sup> TERNA S.p.A., Viale Egidio Galbani 70, 00156 Rome, Italy; giuseppe.pelliccione@gmail.com

\* Correspondence: salvatore.celozzi@uniroma1.it

† These authors contributed equally to this work.

**Abstract:** Fast-front transients play an important role in the insulation design of any power system. When a stroke hits the shield wire or the tower of high-voltage overhead power lines, flashover may occur either along the span or across tower insulators, depending on the relevant voltages and insulation strength. As a result, backflashover may take place from the tower structure to the phase conductor whenever a huge impulse current flows along the tower towards considerably high footing impedances. For these reasons, tower modeling for transients studies is an important step in the insulation design, and also for lower voltage applications, where indirect lightning effects may play a predominant role. However, after decades of research on tower modeling, starting from the 1930s with the first model proposed by Jordan, no consensus has been reached neither on a widely accepted tower model nor on the quantitative effect of the tower models on insulation design. Moreover, the fundamental mechanisms at the base of the transient response of towers and the definition of some fundamental parameters have not been totally clarified yet. The aim of this review is to present the available tower models developed through the years in the power community, focussing mainly on lumped/distributed circuit models, and to help the reader to obtain a deeper understanding of them.

**Keywords:** power system transients; tower model; tower surge impedance; transmission lines



**Citation:** Stracqualursi, E.; Pelliccione, G.; Celozzi, S.; Araneo, R. Tower Models for Power Systems Transients: A Review. *Energies* **2022**, *15*, 4893. <https://doi.org/10.3390/en15134893>

Academic Editor: Theofilos A. Papadopoulos

Received: 31 May 2022

Accepted: 30 June 2022

Published: 4 July 2022

**Publisher's Note:** MDPI stays neutral with regard to jurisdictional claims in published maps and institutional affiliations.



**Copyright:** © 2022 by the authors. Licensee MDPI, Basel, Switzerland. This article is an open access article distributed under the terms and conditions of the Creative Commons Attribution (CC BY) license (<https://creativecommons.org/licenses/by/4.0/>).

## 1. Introduction

Insulation coordination has been a cornerstone of power engineering [1] since the first power systems were developed at the beginning of the twentieth century. Proper insulation coordination in power systems is essential for the quality of the service, long-term durability of operating devices, and reduction in operating costs. IEC [2] and ANSI/IEEE [3,4] standards establish, on a solid theoretical and practical ground, definitions, principles, and rules, providing application guidelines and computational examples. Power systems insulation is exposed not only to normal stresses associated with steady-state conditions (e.g., due to corona effect [5,6]), but also to external and internal overvoltages. External overvoltages occur under lightning discharges, while internal overvoltages are caused by faults and switching operations. For high-voltage (HV) transmission systems, direct strikes to ground wires, towers, or power conductors play a dominant role [7–10], while, at lower voltages, induced lightning overvoltages may also become a threat [11,12].

In this context, accurate modeling of transmission line towers is crucial for insulation design. When the lightning discharge hits the earth wires or towers, the backflashover phenomenon may take place, along with the associated short-circuit fault. Back flashover consists of arcs occurring along the insulator strings of one or multiple phase conductors due to the fast rise of the tower voltage with respect to the phase conductor voltages. In fact, backflashover events may be caused by the transient ground potential rise [13] associated with the lightning current flowing along the tower. Actually, a relevant percentage of outages occurring along HV power lines is due to backflashover [14–17]. As a consequence, tower modeling has been the subject of fervent research, started almost one

century ago [18–21], which is still active [22,23]. However, despite all progress, physical phenomena related to towers may be explained only partially by theoretical approaches, several issues still being deeply debated nowadays.

A large number of models has been developed to analyze the transient behavior of towers subjected to steep-fronted waves due to lightning strikes [24,25]. These models are widely used to assess the basic lightning impulse insulation levels (BIL), relevant to the design of power equipment [26]. Indeed, since typical towers (and sometimes crossarms) cannot be approximated as electrically short lines due to their dimensions, these models require procedures to determine the fundamental distributed parameters [27]. Since the earliest approach by Jordan in the 1930s [21], researchers have proposed new models through the years. What is really significant is that these models differ from each other not only in the proposed equivalent representation of the tower and in the adopted numerical or analytical techniques, but also in the main theoretical assumptions concerning propagation mechanisms along the tower and in the definition of the fundamental parameters. In this regard, for example, the concept of surge impedance is used to describe different quantities in tower analysis, although it is well-defined in electromagnetic textbooks [28]. As confirmed in [29,30], researchers proposed four definitions of surge impedance: three are specified in the time domain (TD) (two are function of time, whereas one is constant), and are tied to the shape of the injected current; the fourth is defined as the Inverse Fourier Transform of the harmonic impedance computed in the frequency domain (FD) [28], and it is dependent on the geometry and on electromagnetic properties of the media.

Numerous approaches have been used to determine these equivalent models. Perhaps all the approaches known in electromagnetics have been used to estimate the impact of voltage and current waves propagation along towers: the time-domain finite-difference method [31,32], the frequency-domain method of moments [33], the partial element equivalent circuit method [34], hybrid electromagnetic codes [35,36], black-box approaches [37], and the frequency-domain finite element method [38]. Additionally, there is a huge number of simple and practical models based on analytical approaches—usually based on magnetostatics [39] or transverse electromagnetic (TEM) transmission line assumptions [31]—that are not as computational heavy as full-wave approaches. This is the reason why these methods are preferred and often employed in network studies, although less accurate. What has been observed is that different models result in different transient responses to transient events [23]. Depending on the tower geometrical characteristics and conductors arrangement, and on the specific choice of its equivalent circuit, different voltages of the tower arms are computed [29], leading to different voltages across the insulators, affecting the probability of occurrence of backflashover and the lightning performance of the line, which also depends on the statistical distribution of lightning current characteristics [40], shielding failure, ground flash density, etc.

The first tower model was proposed by Jordan [21], who modeled the tower as an equivalent single-conductor, uniform, lossless Transmission Line (TL). He assessed the propagation of voltage and current waves by means of the TL characteristic impedance (depending on the geometrical features of the tower), and assumed the propagation velocity to be equal to the speed of light. Despite some works claiming the accuracy of the results obtained with Jordan's expression of the characteristic impedance [35], an error was detected in its derivation, and a revised formula was proposed ([39,41]). Successively, others have proposed equivalent lossless TL models, deriving different expressions for the characteristic impedance. While Wagner and Hileman [42] approximated the tower to a cylindrical structure, Sargent and Darveniza [43] proposed an expression for the characteristic impedance of towers approximated by a conical structure. Later, Chisholm et al. [44,45], with reference to conical, cylindrical, and waisted towers, considered the current to be injected horizontally at the tower top. All these models assume that the tower supports a propagating TEM mode, i.e., the electromagnetic field to be a spherical wave, or that this mode represents the major contribution to the tower response. Other researchers presented non-uniform TL models: Randon et al. [46], Saied et al. [47] and Oufi et al. [48] proposed

modeling the tower as a non-uniform, lossless, exponential TL to be studied in the Laplace domain, with the characteristic impedance varying continuously along the tower. Correia de Barros and Almeida [49,50] investigated the propagation along a non-uniform lossy TL equivalent of the tower in the TD through FDTD methods. The tower is discretised in short sections, allowing to approximate the continuous variation (with an arbitrary expression) of the equivalent characteristic impedance. As for truss towers, De Conti et al. [39], Hara and Yamamoto [51], Ametani et al. [52], and Gutierrez et al. [53,54] modeled the tower as an equivalent uniform, lossless, multiconductor TL (MTL), accounting for the self-characteristic impedance of each leg of the tower and for their mutual coupling (or adopting a fictitious conductor accounting for the four legs). Finally, more recent models divide the tower into multiple sections: each section is represented by the series of an equivalent lossless TL, and a lumped resistive-inductive impedance is introduced to account for attenuation. This models, known as multistory models, have been developed by Ishii et al. [55], Baba et al. [56], and Hashimoto et al. [57]. Other authors proposed further modifications or improvements to reproduce simulated or experimental results [58,59].

A final issue to be highlighted is the importance of the footing tower termination in any transient analysis for insulation purposes. Often, a perfectly conducting ground is considered in order to simplify the analysis considering the tower image. However, the authors considered more realistic, yet complex, terminations considering a dissipative earth [60], a grounding grid at the tower foot [61,62], a grounding grid embedded in a frequency-dependent soil [63,64], and accounting also for the soil ionization effect [65].

This review aims at presenting the state of the art in tower modeling and highlighting that the available models for HV towers conduct large differences in the predicted values of the input impedance and peak voltages at the tower top. Section 2 is devoted to the description of the main typologies of towers for power transmission at high voltages. The different definitions of surge impedance or characteristic impedance are clarified in Section 3. Approaches available in the literature to model the electrical behavior of towers by means of an equivalent circuit are reviewed in Section 4, and classified in models adopting single-conductor TL approximation of the tower, MTL approximation, non-uniform TLs equivalents, or multistory models. The influence of the tower grounding system is assessed in Section 5, along with the most common grounding configurations. Numerical results, comparing the impact of the chosen tower model on the input impedance seen at the tower top, are presented in Section 5. Finally, in Section 6, conclusive considerations and remarks are drawn.

## 2. Towers for HV Applications and Common Conductors Arrangements

Tower design has been developed throughout the years along with the spread of power lines. Their shape and size have been initially influenced by mechanical and electrical requirements. However, due to the more recent attention devoted to the impact of human activities on the environment, towers with new, more compact designs have been put in operation as well.

HV towers may be primarily classified into pole and lattice towers, the former type being rarely used at the highest voltage levels (namely, above 700 kV) [66]. In Figure 1, the most used tower structures and conductor configurations are sketched (not to scale). Lattice towers consist of a main vertical structure, which can be in the shape of a pyramid, or made of two sections, namely, the tower cage and lower body. In the derivation of equivalent circuits to simulate the electrical behavior of such towers, these are frequently approximated to cylinders or cones sharing approximately the same dimension of the actual tower base.

Lateral crossarms are included to support the phase conductors. For single-circuit lines, depending on the path of the line, environmental restrictions, and reduction in the emitted magnetic field at power frequency, crossarms may be located on both sides of the main body (Figure 1a), or on a single side (Figure 1b) (this arrangement being employed where harsher changes in the main direction of the line path want to be achieved).

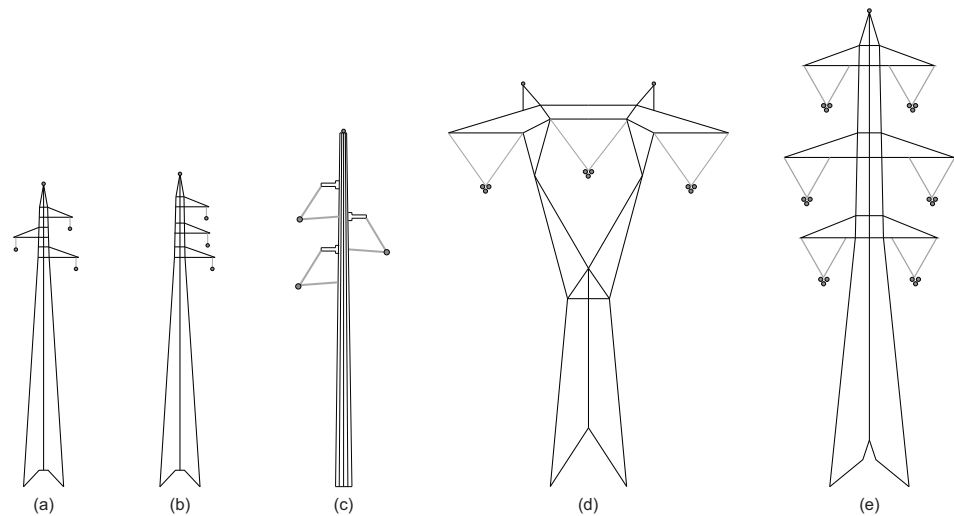


**Figure 1.** Typical towers for HV overhead transmission lines. (a) Single-circuit tower; (b) single-circuit tower with phase conductors located at the right-side; (c) tubular tower with insulating cross-arms; (d) cup-type tower with horizontal arrangement of the phase conductors; (e) double-circuit tower.

Double-circuit lines may be realised by means of six crossarms to support the insulator strings and the corresponding six phase conductors (three at each side of the tower, Figure 1e) [67]. Additional upper crossarms may support two shield wires to protect the line from direct strikes and mitigate the stress on insulators due to induced overvoltages; instead, for single-shield wire configurations, the protecting conductor is installed at the tower peak. Crossarms are steel trussed structures for the majority of the applications; however, more recent designs are spreading with insulating cross-arms, which represent the structural elements supporting the high-voltage conductors and provide the electrical insulation required by the BIL associated to the line. The advantage of the latter configuration consists of a partial reduction in the visual impact of the line and of the right of way, due to the reduced cross-section of the arrangement (in Figure 1c, a tubular tower with insulating cross-arms is represented).

Eventually, cup-type towers (Figure 1d) are employed when the phase conductors need to be located at approximately the same height above the ground. This arrangement is commonly adopted in the proximity of substations, to favor connection of phase conductors to bus-bars, and in areas with strict limitations on the maximum height of neighbouring structures (e.g., in proximity to military areas, airports, etc.).

### 3. Definitions of Surge Impedance and Propagation Constant

Equivalent circuits of transmission line towers proposed in the literature rely on TL models to account for propagation along suitable sections of the tower or along the whole structure. For this purpose, surge impedances and propagation constants are introduced in order to characterize the aforementioned TLs. However, different definitions have been ascribed to the surge impedance [13,28].

Several researchers (e.g., [42,43]) employed the *transient surge impedance*  $z(t)$ , defined in the time domain as the ratio

$$z(t) = \frac{v(t)}{i(t)}, \quad (1)$$

to derive the surge (or characteristic) impedance for TL models, equivalent to the tower under study. In (1),  $v(t)$  is the time-dependent voltage, and  $i(t)$  is the injected current at the tower top. The resulting quantity, with the dimension of an impedance, is a function of time, of the geometrical features of the tower under analysis, and of the excitation current [68]; a step or ramp current is often employed, although different waveforms have been proposed later in the literature ([69,70]) to reproduce realistic lightning currents [71]. Hence, (1) is not suitable to obtain a characterization of the tower, which, being independent of the injected current, should allow to predict the tower response to different excitations.

The value attained by (1) at time  $t^* = 2h_T/c_T$  is adopted as the sought value of characteristic impedance, where  $h_T$  is the height of the tower and  $c_T$  is the surge propagation velocity along the tower.

The reasons underlying this choice are linked to the time necessary for voltage waves reflected at the tower base to reach the tower top; at times  $t < t^*$ , the input impedance seen at the tower top should equal the characteristic impedance (i.e., the inverse Fourier or Laplace transform of the frequency-dependent standard impedance); however, derivation of this value as a voltage-to-current ratio would be possible only in the case of a lossless and uniform TL, i.e., for a constant-valued (resistive), progressive- and frequency-independent characteristic impedance. Indeed, if these simplifying hypotheses do not hold, a time convolution would link the current with the time-domain tower impedance; furthermore, reflections are expected at the tower top at time  $t < t^*$  due to the non-uniformity of the line.

Other approaches rely on the concept of *harmonic impedance*, which is computed in the frequency domain as the ratio

$$z(\omega) = \frac{v(\omega)}{i(\omega)}, \quad (2)$$

where  $v(\omega)$  and  $i(\omega)$  denote voltage and current at the tower top at angular frequency  $\omega$ . The resulting ratio may be alternatively interpreted as the input impedance of the structure, only depending on intrinsic features of the tower [48]. This approach allows us to derive the response, seen at the tower top, to any current excitation, by computing the time domain convolution of the inverse Fourier transform of (2) (i.e., the tower impulse response) with the injected current.

#### Propagation Constant

When referring to lossless TL models, the propagation constant is accounted for only by the phase constant  $\beta = \omega/c_T$ , defined as the ratio of the angular frequency  $\omega$  and  $c_T$ .

Attempts have been made to attribute a suitable value to  $c_T$ , based on experimental activities (Table 1), recognizing that the complexity of measuring methods and arrangements may affect the accuracy of results [72]. A common procedure consists of measuring elapsed time from  $t = 0$  (when a current source is applied at the tower top), and  $t = t^*$  necessary for voltage waves reflected at the tower base to travel upwards and reach the tower peak; hence, surge propagation velocity is computed as  $c_T = 2h_T/t^*$ . Actually,  $c_T$  corresponds to a mean velocity, and it is subsequently employed in numerical simulations assuming that the surges travel along the tower at a constant speed  $c_T \leq c_0$  ( $c_0$  denotes the speed of light).

**Table 1.** Common values of surge velocity deduced from experimental activities to assess propagation along transmission line towers.

Authors	Ref.	Experimental Arrangement	Height [m]	$c_T/c_0$ [p.u.]
Breuer et al.	[73]	HV tower, vertical conductors	51 44	0.95–0.96
Ishii et al.	[55]	HV tower	62.8	$\simeq 1$
Kawai et al.	[72]	HV tower	26–214	0.7–0.88
Motoyama et al.	[74]	Reduced-scale model HV tower UHV tower	3 48.2 120	0.8–0.87
Chisholm et al.	[45]	Reduced-scale smooth cone	0.4	$\simeq 1$
Chisholm et al.	[75]	HV towers	25.5–57.0	0.96–1
Motoyama et al.	[76]	HV tower	89.5–94.5	0.85–0.9
Noda	[60]	HV tower	77	0.92

#### 4. Tower Models

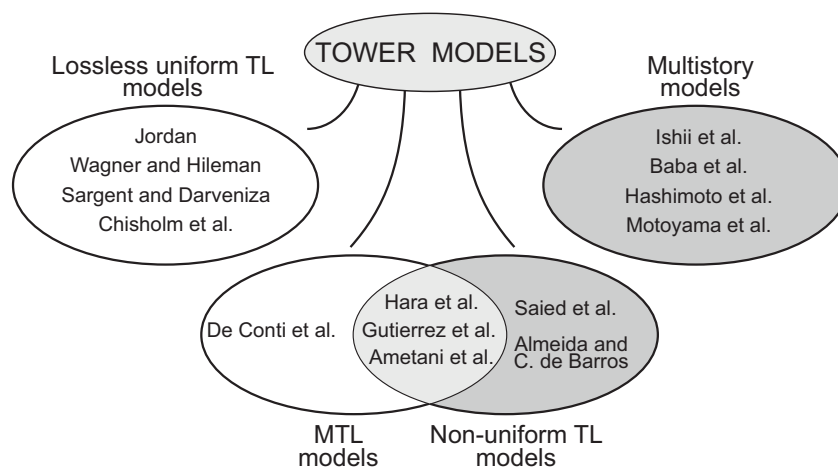
Approaches and expressions proposed in the literature to simulate the electrical response of transmission towers (in Tables 2 and 3) have been classified into four categories: lossless uniform TLs, MTLs, multistory models, and non-uniform TLs. These models mainly adopt a distributed parameter equivalent circuit for the tower, defining the fundamental quantities of an equivalent TL, i.e., propagation constant and characteristic impedance. However, the categorization proposed here should not be intended to be strict. Indeed, this accounts for the fundamental aspects of each reviewed model; nevertheless, some of the approaches may belong to several groups of the following classification. Figure 2 displays a syntectic diagram, which accounts for the classification introduced in the present review, and the main reviewed models.

**Table 2.** Relevant tower models proposed in the literature (I).

Model	Type	Main Features	Equivalent	Soil Effect
Jordan [21,39,41]	Lossless uniform TL	Based on magnetostatics principles and low-frequency approximations.	Cylindrical	×
Wagner and Hileman [42]	Lossless uniform TL	Derived in the time domain by loop-voltage method and Kirchoff's current law. The characteristic impedance is assumed equal to the value attained by the transient surge impedance at $t = 2h_T/c_0$ .	Cylindrical	×
Sargent and Darveniza [43]	Lossless uniform TL	Analysis developed in the time domain. Characteristic impedance computed as the value attained at $t = 2h_T/c_0$ by the ratio of the tower top voltage (integral of the electric field, neglecting the effect of the scalar electric potential) over the injected current.	Cylindrical Conical	×
Chisholm et al. [44,45]	Lossless uniform TL	Accounting for horizontal direction of current injection at the tower top. Derived by application of theory of biconical TLs.	Cylindrical Conical	×
De Conti et al. [39]	Lossless MTL	MTL model based on magnetostatics principles and per unit length inductances computation.	Cylindrical	×
Hara and Yamamoto [51]	Lossless TL	Cascade of parallel lossless TLs (with empirical characteristic impedances) accounting for the legs and bracing. The four main legs of the tower are reduced to a simple TL through an equivalent radius. Additional lossless, horizontal TLs account for the arms.	Cylindrical	×
Ametani et al. [52]	MTL	Computation of a potential coefficient matrix for each tower section accounting for current images with respect to a reference plane at complex depth. The tower is modeled by a cascade of multiconductor (or single-conductor with an equivalent radius) TLs.	Cylindrical	✓
Ishii et al. [55] Baba et al. [56]	Multistory model	Cascade of lossless TLs and damping resistive-inductive elements. Values of the characteristic impedances are derived empirically.	-	×
Hashimoto et al. [57]	Multistory model	Cascade of TLs and damping resistive-inductive elements, with an additional capacitance-to-ground at the tower top. Values of the characteristic impedances and lumped elements are derived to reproduce available experimental data for the system consisting in a tower equipped with power-line conductors.	-	×

**Table 3.** Relevant tower models proposed in the literature (II).

Model	Type	Main Features	Equivalent	Soil Effect
Motoyama et al. [58]	Multistory model	Cascade of TLs and damping resistive-inductive elements. Values of the characteristic impedances are derived empirically.	-	×
Gutierrez et al. [53]	Non-uniform TL	Non-uniform MTL (or single conductor equivalent) with characteristic impedances given by the ratio of the voltage (computed as the integral of the electric field in the polar direction produced by a bipolar antenna with vertex lying on a reference plane at complex depth) and the source current.	Cylindrical	✓
Saied et al. [47]	Lossless non-uniform TL	Cylindrical exponential TL model, with progressive-dependent characteristic impedance (starting from assumed values at relevant heights).	Cylindrical	×
Almeida and Correia de Barros [49]	Non-uniform TL	Progressive-dependent characteristic impedance (starting from assumed values at the tower top and base). Propagation assessed by means of FDTD methods and possible inclusion of frequency-independent per unit length losses.	Cylindrical	×

**Figure 2.** Classification of the reviewed circuit models for transmission line towers [21,39,42,43,45,47,49,51–53,55–58].

#### 4.1. Lossless Uniform Transmission Line Models

The tower is typically represented by a cascade of equivalent lossless TLs (sharing the same characteristic impedance), each corresponding to a tower section, as in Figure 3; indeed, the tower is suitably divided into sections to ease the computation of arms voltages, and, eventually, of voltages across the insulators. Expressions for the tower characteristic impedance are often derived considering towers located over a perfectly conducting plane (PEC), after being reduced to an equivalent cylinder or cone.

These models assume that the electromagnetic field associated with sources at the top of the tower propagates with the characteristic pattern of spherical waves; hence, the tower is assumed to support a propagating TEM mode, studied by means of an equivalent TL with constant characteristic impedance and propagation velocity.

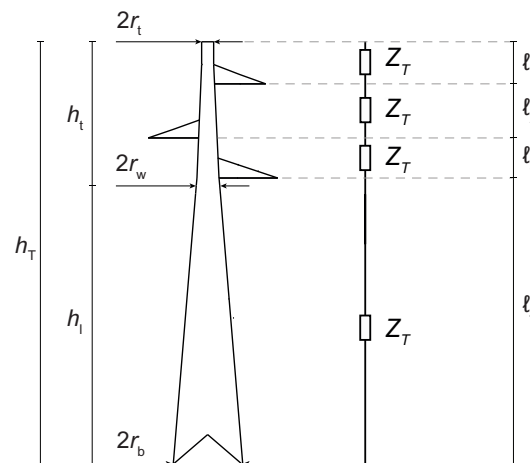


**Figure 3.** Cascade of uniform and lossless transmission lines modeling the corresponding sections in which the tower is subdivided.

#### 4.1.1. Jordan Model

One of the first tower models was proposed by Jordan [21]. The travelling surges are assumed to propagate along the tower structure at the speed of light, the tower being represented by a uniform, lossless TL with propagation constant  $\beta_0 \simeq \omega/c_0$  and characteristic impedance given by

$$Z_T = 60 \ln\left(\frac{h_T}{r_e}\right) + 90 \frac{r_e}{h_T} - 60. \tag{3}$$

In (3),  $h_T$  denotes the height of the tower. However, several authors (e.g., [39,41]) have revised expression (3), claiming that an error was committed by Jordan in the first place, in favor of the following:

$$Z_T = 60 \ln\left(\frac{4h_T}{r_e}\right) - 60. \tag{4}$$

In particular, expressions (3) and (4) only depend on the tower height and equivalent radius, denoted by  $r_e$ . As for the choice of the tower equivalent radius  $r_e$ , it is often considered equal to the radius at the tower base, or computed as a weighted average of the radii of cross-sections of the tower located at different heights from the ground [77].

The expression of the characteristic impedance is derived as follows: the magnetic vector potential at an observation point  $P$ , located on the surface of the equivalent cylinder, is due to a current  $I$ , which flows in a vertical channel corresponding to the cylinder axis and extending from  $h = 0$  to  $h = h_T$  over a PEC plane; the influence of the PEC plane is taken into account by application of the theory of perfect images, considering the contribution of the image current extending from  $h = -h_T$  to  $h = 0$ ; accordingly, the flux  $\Phi_T$  of the magnetic induction field through the surface  $S$  in Figure 4 is derived as

$$\Phi_T = L_T I = \frac{\mu_0 I}{4\pi} \int_0^{h_T} \int_0^{h_T} \left[ \frac{1}{\sqrt{(x-x')^2 + r_e^2}} + \frac{1}{\sqrt{(x+x')^2 + r_e^2}} \right] dx' dx. \tag{5}$$

In (5),  $L_T$  denotes the tower inductance. The vertical component  $A_x$  of the magnetic vector potential is obtained by means of the inner integral, superimposing the contributions from the vertical current dipoles located from 0 to  $h_T$  (and their corresponding images). Subsequently, the circulation of  $A_x(x, y)$  (i.e., the sought flux) is computed by means of the external integral with reference to the integration path in Figure 4; indeed, with  $A_x$  being the only component of the magnetic vector potential, integration along the horizontal sections of the path does not contribute to the circulation; the same holds for the vertical path at infinite distance, where  $A_x$  is considered to vanish.



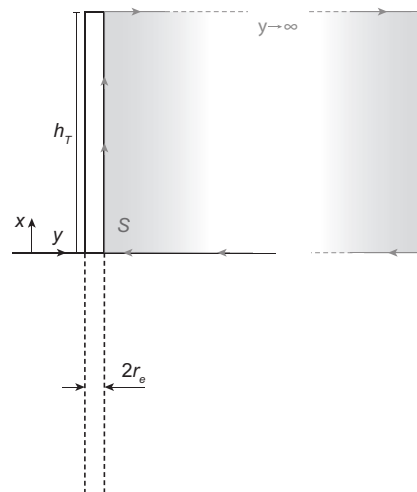


**Figure 4.** Reference vertical cylinder over a PEC plane for the computation of the characteristic impedance according to the revised Jordan model.

If the tower in Figure 4 is modeled as a uniform lossless TL with short-circuited termination (corresponding to the PEC plane configuration), the following can be written:

$$Z_{in} = Z_T \tanh\left(j\frac{\omega}{c_0}h_T\right) \simeq j\frac{\omega}{c_0}h_T Z_T = j\omega L_T. \quad (6)$$

In (6), an approximation of the input impedance  $Z_{in}$  seen at the tower top at low-frequency and/or for small  $h_T$  is displayed as a function of the tower characteristic impedance  $Z_T$ ; this approximated quantity should correspond to the reactance associated to  $L_T$  in (5). Hence, the adopted low-frequency approximation allows to obtain easily  $Z_T = c_0 L_T / h_T$ .

The previous derivation deserves some relevant clarifications. The complex tower structure, even if only the four main legs are considered, is reduced to an equivalent vertical cylinder; the current is assumed to flow orthogonally to the PEC plane. Hence, the computed magnetic induction field neglects the contribution deriving from the actual incline of the tower structural elements. A second remark regards (5); indeed, this expression is derived assuming the vertical dipoles to carry the same current  $I$ , neglecting any phase variation in the current due to the propagation along the cylinder. This last aspect reveals that the proposed model is based on a low-frequency assumption and magnetostatics principles.

#### 4.1.2. Wagner and Hileman Model

According to this approach, the tower is approximated by a cylinder of radius  $r_e = r_1$  equal to the one at the tower base in Figure 5b; the influence of the soil with finite conductivity is neglected.

Wagner and Hileman originally proposed an expression for the *transient surge impedance*, i.e., a time-dependent quantity:

$$z_T(t) = 60 \ln\left(\sqrt{2}\frac{c_0 t}{r_e}\right). \quad (7)$$

The derivation of (7) (which can be found in Appendix I of [42]) is based on the loop-voltage method, with reference to the injected rectangular current wave being split into the current flowing through the tower  $I_T(t)$ , and the currents flowing along the shield wire in two opposite directions  $I_s(t)$ . The retardation effect due to the finite propagation speed of traveling waves along the tower and shield wire was accounted for in the computation of the electric field (hence, of the voltage drops of interest). An approximation is made, computing the tower transient impedance as the ratio of the voltage at the tower peak over

the current  $I_T$ . With reference to a lightning current with rectangular waveshape, the tower characteristic impedance is approximated to the value assumed by (7) at time  $t = 2h_T/c_0$ :

$$Z_T = 60 \ln \left( \sqrt{2} \frac{2h_T}{r_e} \right). \quad (8)$$

The traveling waves propagation speed is set equal to the speed of light  $c_0$ .

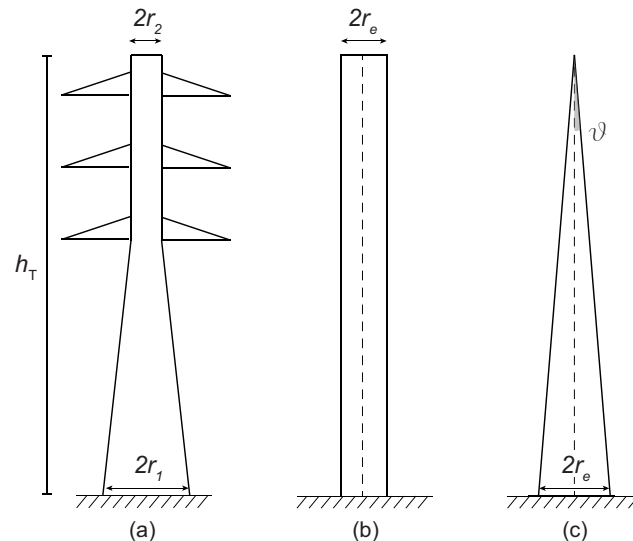


**Figure 5.** Different equivalent structures considered for the tower under study; (a) Tower under study; (b) Approximated cylindrical equivalent tower; (c) Approximated conical equivalent tower.

The derivation of the electric field and transient surge impedance follows the approach presented in [78], based on field theory. However, several assumptions are made: the current along the tower is assumed to flow along the axis of an equivalent vertical cylinder; the effect of static charges is neglected, i.e., only the contribution of the magnetic vector potential caused by the current flowing along the tower is considered when evaluating the electric field; although the procedure to consider multiple current reflections at the ground plane (namely, a PEC plane) and at the tower top is given in the time domain, the chosen value for the characteristic impedance in (8) is computed at time  $t = 2h_T/c_0$ , i.e., it does not account for these reflected waves. Furthermore, the expression was first derived assuming for the current components flowing along the tower and the shield wire to keep the same shape of the injected step current (which cannot be considered an assumption of general validity).

#### 4.1.3. Sargent and Darveniza Model

An expression for the transient surge impedance was proposed for a ramp current being injected at the top of a tower (cylindrical equivalent) [43].

$$Z_T(t) = 60 \left[ \ln \left( \sqrt{2} \frac{c_0 t}{r_e} \right) - 1 + \frac{r_e}{2c_0 t} + \left( \frac{r_e}{2c_0 t} \right)^2 \right] \quad (9)$$

The transient surge impedance (9) was derived in the time domain, adopting  $c_0$  as the propagation speed of voltage and current waves; the top-to-base voltage drop on the surface of the cylinder is evaluated by integration of the electric field, which is derived as the time derivative of the vector magnetic potential.

As for towers presenting an upper cylindrical body and lower truncated conical shape, the equivalent radius  $r_e$  of the cylinder approximating the whole body is computed by means of an empirical expression [79]:

$$\ln(r_e) = \frac{1}{r_1 - r_2} \{r_1[\ln(r_1) - 1] - r_2[\ln(r_2) - 1]\}, \quad (10)$$

where  $r_1$  and  $r_2$  in Figure 5 are the radii at the tower base and at the tower top, respectively. The characteristic impedance  $Z_T$  is computed as the value attained by (9) at  $t = 2h_T/c_0$ :

$$Z_T = 60 \left[ \ln \left( \sqrt{2} \frac{2h_T}{r_e} \right) - 1 + \frac{r_e}{4h_T} + \left( \frac{r_e}{4h_T} \right)^2 \right] \quad (11)$$

which, for  $h_T \gg r_e$ , reduces to

$$Z_T \simeq 60 \ln \left( \sqrt{2} \frac{2h_T}{r_e} \right) - 60. \quad (12)$$

In [43], it is shown that (11) is consistent with expression (8) proposed by Wagner and Hileman. In fact, (11) can be retrieved by application of the Duhamel's integral to compute the response of the tower to a ramp current, assuming its known initial response to be expressed by (7).

When the tower is approximated by a conical structure, the radius  $r_e$  is chosen in the range of the radii of the inscribed and circumscribed circumferences at the tower base. The same derivation, based on the computation of the voltage drop along the tower as the line integral of the electric field on the surface of the cone (derived from the computed magnetic vector potential), leads to the following expression for the characteristic impedance (with reference to a step current injected at its top):

$$Z_T = 60 \ln \left( \frac{\sqrt{2}}{S} \right), \quad (13)$$

where  $S = \sin(\theta)$ ;  $\theta$  is the half-angle of the cone in Figure 5c. In [43], it is observed that the characteristic impedance of a cone does not depend on the waveshape of the injected current, since (13) is constant-valued and time-independent.

The same approach presented by Lundholm et al. in [78] is exploited to compute the electric field. The approximations discussed in Section 4.1.2 for the computation of the electric field and the approach by Lundholm et al. are adopted also in the derivation of (12) and (13). The expressions proposed for the characteristic impedance neither accounts for the soil nor for a PEC plane at the tower base.

#### 4.1.4. Chisholm et al. Model

Several authors have observed discrepancies in the responses of towers for different directions of current injection at the top. Chisholm et al. [44,45] proposed expressions for the characteristic impedance associated with towers with cylindrical, conical, or waisted shape when the lightning current is injected horizontally into the tower top, i.e., in the direction parallel to the ground plane. The tower is approximated by a conical equivalent, and the corresponding characteristic impedance is derived from the theory of biconical TLs with perfectly conducting walls [80], fed horizontally at the cone vertex. Indeed, to account for horizontally injected currents, the tower is modeled as a cone with the vertex lying on a PEC plane; its characteristic impedance  $Z_T$  is derived from the constant valued characteristic impedance  $Z_B$  of the biconical TL in Figure 6 when  $\theta_2 = \pi/2$  (angles  $\theta_1$  and  $(\pi - \theta_2)$  determining the aperture of the upper and lower cone in Figure 6a, respectively):

$$Z_B = \frac{\eta_0}{2\pi} \ln \left[ \frac{\cot(\theta_1/2)}{\cot(\theta_2/2)} \right] \xrightarrow{\theta_2=\pi/2} Z_T = 60 \ln \left[ \cot \left( \frac{\tan^{-1}(r_e/h)}{2} \right) \right] \quad (14)$$

where  $\eta_0 = \sqrt{\mu_0/\epsilon_0}$  is the characteristic impedance in vacuum and  $r_e$  is the radius at the tower base. It is evident that (14) does not depend on the distance from the cone vertex;

indeed, the structure presents a constant characteristic impedance and can be modeled as a uniform lossless TL.

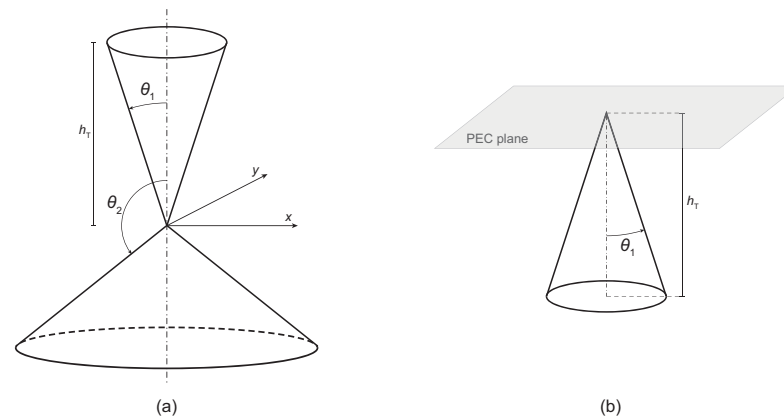


**Figure 6.** Biconical transmission line, used to approximate a conical tower with horizontal direction of current injection at its apex. (a) Generic biconical transmission line; (b) Biconical transmission line for tower application, with  $\theta_2 = \pi/2$ .

For cylindrical towers and horizontally injected current, the following expression is proposed for  $Z_T$  [45]:

$$Z_T = 60 \ln \left[ \cot \left( \frac{\tan^{-1}(r/h)}{2} \right) \right] - 60. \quad (15)$$

As for waisted towers, the characteristic impedance proposed is (for horizontal direction of current injection)

$$Z_T = 60 \ln \left[ \cot \left( \frac{\tan^{-1}(T)}{2} \right) \right] \quad (16)$$

with

$$T = \frac{r_t h_t + r_w (h_l + h_t) + r_b h_l}{(h_l + h_t)^2}, \quad (17)$$

where the quantities  $h_t$ ,  $h_l$ ,  $r_t$ ,  $r_w$ , and  $r_b$  correspond to the heights and radii of the main tower sections as depicted in Figure 3.

Expressions (14)–(16) were proposed to account for lightning currents hitting the shield wire along the span, and resulting in an approximate horizontal direction of the portion of the lightning current reaching the grounded towers. Expression (16) is also adopted in [81], along with a reduced value of the propagation speed  $c_T = 0.8c_0$  accounting for the longer path to the ground caused by the tower bracings and crossarms.

#### 4.1.5. Remarks

Baba and Rakov addressed the assumption of constant characteristic impedance for the tower, whenever approximated by a conical structure over a PEC plane (Figure 7a) [82]. The authors state that this approximation may be used only as long as reflected waves at the base do not reach the tower top. The application of an FDTD method to solve the electromagnetic field in the proximity of a simulated scaled cone showed that propagating waves are attenuated when traveling from the base towards the apex, and that the approximation of spherical field is not accurate after reflection. Hence, the uniform, lossless TL approach only holds for waves traveling towards the tower base, and a non-uniform TL should be exploited to address reflected waves traveling towards the apex (as shown in Figure 7b). Indeed, the incongruence had been already detected, and it was accounted for through an apparent grounding impedance  $Z_{ga}$  (Figure 7c), simulating a partial attenuation of reflected waves through a lumped element, and fictitiously altering the reflection coefficient at the tower base (although conflicting with the unitary reflection coefficient expected at the PEC plane interface). Bermudez et al., from reduced-scale experiments on two

copper horizontal planes tangent to apex and base of a copper cone, proposed an apparent grounding resistance equal to the constant value of  $60 \Omega$  [83]; Chisholm et al. introduced an apparent footing inductance [45].

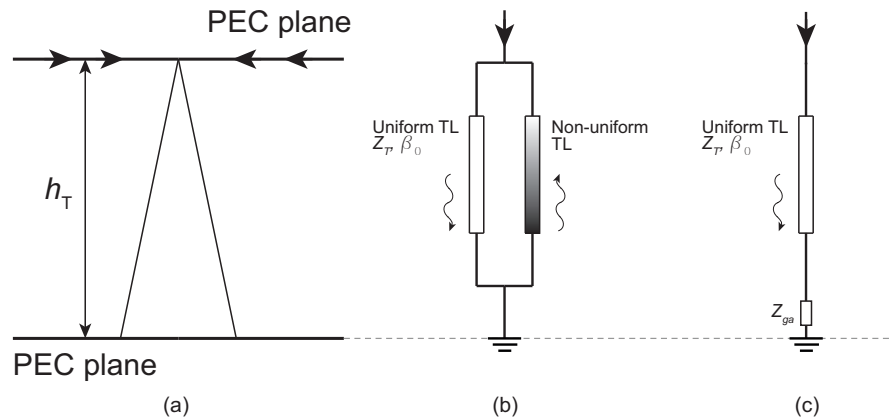


**Figure 7.** Cone approximation of a transmission tower with current injected horizontally at the top. (a) Simplified model; (b) Equivalent transmission line model, as proposed by Baba and Rakov [82] including a non-uniform transmission line to account for reflected waves and non-spherical reflected field; (c) equivalent uniform transmission line model proposed in [75,83] including a fictitious ground plane impedance  $Z_{ga}$ .

#### 4.2. Multiconductor Transmission Line Models

##### 4.2.1. De Conti et al. Model

De Conti et al. [39] proposed an extension to Jordan’s approach, in order to model truss towers as MTLs, consisting of four conductors (namely, the tower legs). In particular, the self characteristic impedance of each leg is computed as illustrated in Section 4.1.1, i.e., through the revised Jordan formula (4), where  $r_e$  is replaced by  $r_c$  (denoting the radius of the tower legs).

The mutual characteristic impedance  $Z_{M,ij}$  between legs  $i$  and  $j$  ( $i, j = 1, \dots, 4$ ) is computed by the evaluation of the vertical component of the magnetic vector potential  $A_x$  produced on the axis of leg  $i$  by the current flowing along leg (and image)  $j$  (under the assumption  $r_c \ll d_{ij}$ ), and by the subsequent integration of  $A_x$  between  $x = 0$  and  $x = h_T$ :

$$Z_{M,ij} = 60 \ln \left( \frac{2h_T + \sqrt{4h_T^2 + d_{ij}^2}}{d_{ij}} \right) + 30 \frac{d_{ij}}{h_T} - 60 \sqrt{1 + \frac{d_{ij}^2}{4h_T^2}}. \tag{18}$$

In (18),  $d_{ij}$  is the distance between the axis of conductors  $i$  and  $j$  (as shown in Figure 8). The same low-frequency assumptions discussed in Section 4.1.1 are made. Characteristic impedances are derived with a PEC surface and application of the perfect image theory;  $c_0$  is adopted as the propagation speed of travelling waves.

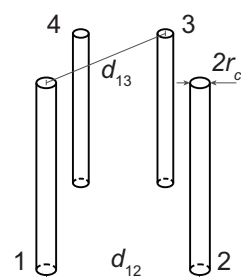


**Figure 8.** System of four parallel vertical conductors approximating the main legs of the truss tower under study.

#### 4.2.2. Hara and Yamamoto Model

Hara and Yamamoto ([51], in Japanese) proposed an empirical expression for the characteristic impedance of a generic vertical conductor with radius  $r$  and height  $h_T$  over a PEC plane:

$$Z_S = 60 \left[ \ln \left( \frac{2\sqrt{2}h_T}{r} \right) - 2 \right], \quad (19)$$

Expression (19) was derived from experimental activity. A steep-front current was injected at the top of vertical conductors (with different radii and heights) over a PEC surface, and the characteristic impedance was computed as the ratio of the measured voltage over current at the injection point for  $t = 2h_T/c_T$  (with  $c_T \simeq c_0$ ).

If  $r$  is replaced by an equivalent radius  $r_e$  accounting for a system of  $n$  vertical conductors, the  $n$  tower legs are reduced to an equivalent single-conductor.

In [84], the originally developed model was extended to account for the effect of the tower bracing and crossarms; the tower body is divided into  $N_s$  segments. The reference tower in Figure 9 is divided into four sections ( $N_s = 4$ ); each section is represented by the equivalent circuit depicted in Figure 9, consisting of two parallel TLs. The TLs corresponding to characteristic impedances  $Z_{T_i}$  should simulate propagation along an equivalent single conductor accounting for the four legs; the TLs represented by characteristic impedances  $Z_{B_i}$  account for propagation along the tower bracings. However, the length of the former TLs is set to  $\ell_i$  in Figure 9, while the length  $\ell_{B_i}$  of the latter ones, corresponding to the bracings, is increased by a factor 1.5, i.e.,  $\ell_{B_i} = 1.5\ell_i$ , to simulate the longer path of currents towards ground. The characteristic impedances are computed as follows:

$$Z_{T_i} = 60 \left[ \ln \left( \frac{2\sqrt{2}h_i}{r_{e_i}} \right) - 2 \right] \quad (20a)$$

$$Z_{B_i} = 9Z_{T_i}, \quad (20b)$$

while  $\beta_0 = \omega/c_0$  is considered as the propagation constant for both TLs and arms. In (20),  $i = 1, \dots, N_s$ , and the quantity  $r_{e_i}$  is the equivalent radius of the  $i$ th section of the tower. For the tower with square cross section in Figure 9,  $r_{e_i}$  is computed as:

$$r_{e_i} = \sqrt[4]{r_i d_i^3 \sqrt{2}} = 2^{(1/8)} \left( r_{T_i}^{(1/3)} r_B^{(2/3)} \right)^{1/4} \left( d_{T_i}^{1/3} d_B^{2/3} \right)^{3/4} \quad (21)$$

with

$$r_i = r_{T_i}^{1/3} r_B^{2/3} \quad (22a)$$

$$d_i = d_{T_i}^{1/3} d_B^{2/3}. \quad (22b)$$

$r_B$  and  $d_B$  correspond, respectively, to the radius of each leg and to the distance between adjacent legs at the tower base, and  $r_{T_i}$  and  $d_{T_i}$  are the corresponding quantities measured at  $h = h_i$  in Figure 9. Expression (21) corresponds to a geometrical mean of mutual distances between the tower legs belonging to the  $i$ th section.

The  $k$ th tower arm is modeled by means of a horizontal TL (connected to the TL equivalent of the tower body) with length equal to the arm length, characteristic impedance  $Z_{A_k}$  and propagation constant  $\beta_0$ :

$$Z_{A_k} = 60 \ln \left( \frac{2h_k}{r_{A_k}} \right); \quad (23)$$

$k$  ranges from 1 to the total number of arm pairs,  $h_k$  and  $r_{A_k}$  are, respectively, the arm height and equivalent radius (to be approximated as 1/4 of the width of the arm at the tower side).

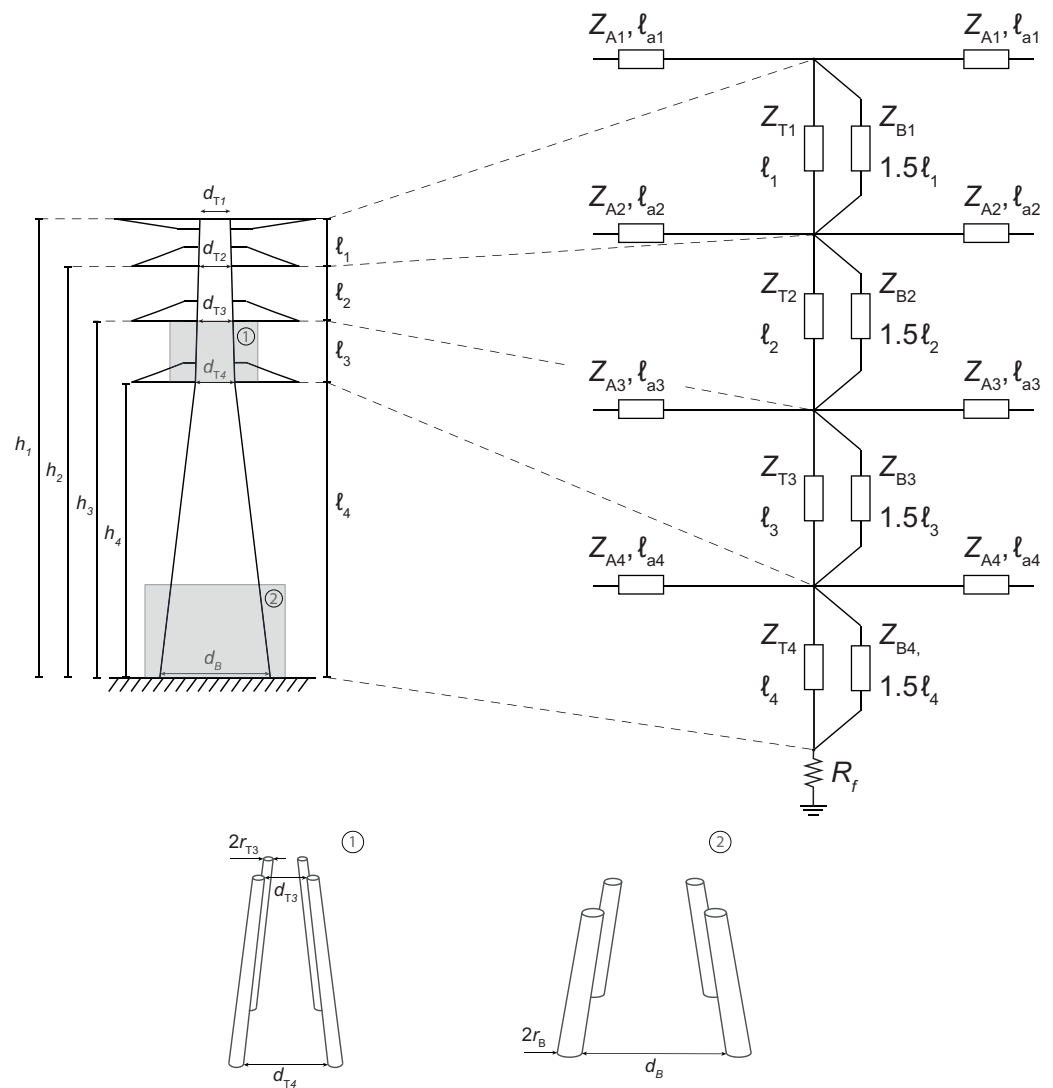


**Figure 9.** Equivalent circuit proposed by Hara and Yamamoto [84], partitioning the tower in  $N_s = 4$  sections; suitable transmission lines account for the tower main body ( $Z_{T_i}, \beta_0$ ), bracings ( $Z_{B_i}, \beta_0$ ), and crossarms ( $Z_{A_i}, \beta_0$ ).

It should be noted that the approach by Hara et al. might be classified as a non-uniform TL model as well, due to the assumed dependence of  $Z_{T_i}$  on the height of section  $i$  over the reference ground.

#### 4.2.3. Ametani et al. Model

Ametani et al. [52] proposed to model the tower as a cascade of MTLs, each of them consisting of four parallel vertical conductors above the ground plane. An approach based on Neumann’s integral, similar to the one presented in Section 4.1.1 for the derivation of the characteristic impedance by Jordan, is adopted. However, the contribution of the image conductors accounts for the finite conductivity of the ground by moving the reference plane at zero potential at a complex depth  $h_c = \sqrt{\rho_g / (j\omega\mu_g)}$  (where  $\rho_g$  and  $\mu_g$  are the ground electric resistivity and magnetic permeability, respectively) [85]. The reference configuration for two conductors above the ground with resistivity  $\rho_g$  is depicted in Figure 10.

The matrices of per unit length (p.u.l.) inductances and capacitances for the multiconductor system in Figure 11b (namely, a tower section) are given by:

$$\mathbf{C} = 2\pi\epsilon_0\mathbf{P}_0^{-1} \tag{24a}$$

$$\mathbf{L} = \frac{\mu_0}{2\pi}\mathbf{P}, \tag{24b}$$

where  $\mathbf{P}/(2\pi\epsilon_0)$  is the potential coefficient matrix; the notation  $\mathbf{P}_0$  is adopted to refer to  $\mathbf{P}$  when it is computed in the case of PEC ground (i.e., for  $h_c \rightarrow 0$ ). Expressions of the elements  $P_{ij}$  of the matrix  $\mathbf{P}$  may be found in [52], and are computed as

$$P_{ij} = \frac{M_{ij} + M'_{ij}}{2\ell} \tag{25}$$

with  $\ell = h_t - h_b, i, j = 1, \dots, 4$ , and

$$M_{ij} = \int_{h_b}^{h_t} \int_{h_b}^{h_t} \frac{dx_i dx_j}{\sqrt{d_{ij}^2 + (x_i - x_j)^2}} \tag{26a}$$

$$M'_{ij} = \int_{h_b}^{h_t} \int_{-h'_b}^{-h'_t} \frac{dx_i dx'_j}{\sqrt{d_{ij}^2 + (x_i - x'_j)^2}}. \tag{26b}$$

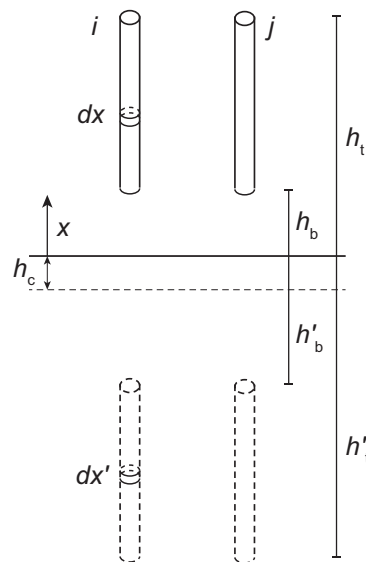


**Figure 10.** Two vertical conductors (approximating two legs of the tower) extending from  $h = h_b$  to  $h = h_t$  over the soil; the finite conductivity of the soil is accounted for through an equivalent configuration, which includes the conductors' images with respect to an auxiliary plane at reference potential, placed at complex depth  $h_c$  below the soil-air interface.

The element  $P_{ij}$  may be expressed as follows:

$$P_{ij} = \log \left\{ \frac{[\sqrt{d_{ij}^2 + \ell^2} + \ell][\sqrt{d_{ij}^2 + (H - 2\ell)^2} + H - 2\ell]}{d_{ij}[\sqrt{d_{ij}^2 + (H - \ell)^2} + H - \ell]} \right\} +$$

$$+ \left(\frac{H}{2\ell}\right) \log \left\{ \frac{[\sqrt{d_{ij}^2 + (H - \ell)^2} + (H - \ell)]^2}{[\sqrt{d_{ij}^2 + H^2} + H][\sqrt{d_{ij}^2 + (H - 2\ell)^2} + H - 2\ell]} \right\} +$$

$$+ \left(\frac{1}{2\ell}\right) \left\{ 2d_{ij} + \sqrt{d_{ij}^2 + H^2} + \sqrt{d_{ij}^2 + (H - 2\ell)^2} - 2\sqrt{d_{ij}^2 + \ell^2} - 2\sqrt{d_{ij}^2 + (H - \ell)^2} \right\}. \tag{27}$$



where  $H = 2(h_t + h_c)$  and  $d_{ij}$  is the distance between the axis of conductor  $i$  and  $j$  in Figure 11. In (26) and (27),  $d_{ij} = r_c$  should be adopted when computing self-terms of the matrix  $\mathbf{P}$  (i.e.,  $P_{ij}$  for  $i = j$ ).

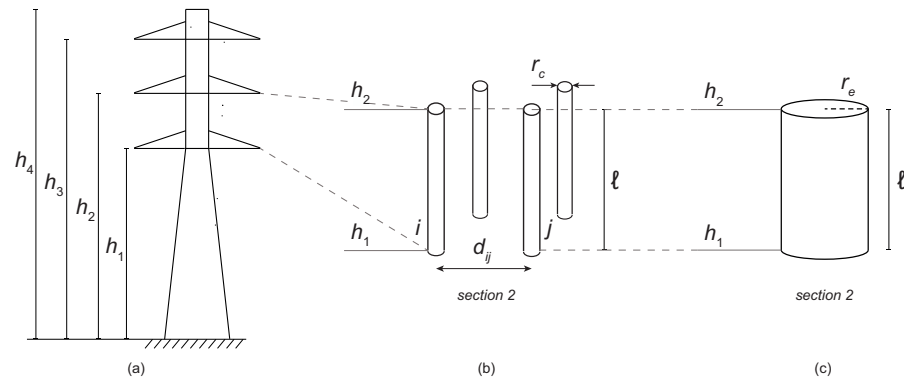


**Figure 11.** Set of four parallel vertical conductors to be modeled as an equivalent single conductor transmission line according to Ametani et al. [52]; (a) Transmission tower partitioned into sections; equivalent four-conductors system (b) and equivalent single-conductor model (c) of the considered section (section 2 in the figure).

The matrices of p.u.l. inductances and capacitances, computed above, are employed to derive the matrices of propagation constants  $\Gamma$  and characteristic impedances  $\mathbf{Z}_T$  through standard MTL analysis. For the PEC plane case the following expressions hold:

$$\Gamma^2 = -\omega^2 \mathbf{L}_0 \mathbf{C}_0 \quad (28)$$

$$\mathbf{Z}_T = 60 \mathbf{P}_0. \quad (29)$$

However, propagation along the system of four conductors can be assessed also by means of an equivalent single-conductor TL with characteristic impedance

$$Z_T = (Z_{T11} + 2Z_{T12} + Z_{T13})/4 \quad (30)$$

or computing the characteristic impedance of the TL associated with an equivalent conductor of radius  $r_e$ :

$$r_e = \left( r_c \sqrt{2d_{ij}^3} \right)^{\frac{1}{4}}. \quad (31)$$

Relevant geometrical quantities referred to in this section are shown in Figure 11;  $r_c$  is the radius of each tower leg, and  $d_{ij}$  is the mutual distance between the axis of leg  $i$  and  $j$ .

The three proposed solutions (i.e., MTL equivalent, single-conductor TL reduction, and TL associated to a single conductor with an equivalent radius) may be exploited to characterize different sections of the tower (e.g., section  $i$  extending from  $h_{b_i} = h_{i-1}$  to  $h_{t_i} = h_i$ ). The tower is modeled by a cascade of TLs with different characteristic impedances (i.e., as a non-uniform MTL), depending on the height and on the mutual distance between the tower legs of the section (an exact definition of the latter quantity is not given to reduce the four leaning legs to a system of four parallel conductor).

For  $h_b = 0$  and the PEC plane, the expression of the characteristic impedance coincides with the one originally proposed by Jordan; hence, the orientation of the current images in [52] may have been incorrectly chosen in the opposite direction with respect to the real current flowing along the conductor above the ground plane [39].

Results presented in Section 5 refer to the implementation of the approach as originally proposed by Ametani et al.; the tower is approximated by a single-conductor TL with equivalent radius given by (31); the following relations are implemented to derive the

propagation constant  $\Gamma(\omega)$  and characteristic impedance  $Z_T(\omega)$  when the lossy ground is considered:

$$C = 2\pi\epsilon_0 P_{0,ii}^{-1} \tag{32a}$$

$$L = \frac{\mu_0}{2\pi} P_{ii} \tag{32b}$$

$$\Gamma(\omega) = \sqrt{-\omega^2 LC} \tag{32c}$$

$$Z_T(\omega) = \sqrt{L/C} . \tag{32d}$$

Expression (32) depends on the height above the ground and equivalent radius of the considered tower section (indeed, it is derived from (27) for  $i = j$ ); hence, (32) may be used to derive the p.u.l. parameters, propagation constant, and characteristic impedance associated to the chosen tower sections by considering their equivalent radius, length, and height above the ground. In (32a), the PEC plane approximation is adopted in the derivation of the p.u.l. capacitance to ground. The same limitations highlighted in Section 4.1.1 apply to the Ametani et al. model, since it shares common theoretical basis and assumptions.

### 4.3. Multistory Models

Multistory approaches divide the tower into multiple sections (stories), which are modeled by the cascade of a lossless TL and a lumped circuit (its resistive component accounting for attenuation of traveling waves). The tower partitioning is usually meant to provide suitable breaking points along the tower in order to derive voltages at the crossarms.

A feature, common to multistory models, consists of adopting electrical quantities (employed for the tower equivalent circuit), which depend on the story length, but not on the cross-sectional dimensions of the tower under analysis. Depending on their values, a mismatch between adjacent segments may occur, resulting in multiple reflections of travelling waves.

#### 4.3.1. Ishii et al. Model

The tower is divided into  $N_s$  sections ( $N_s = 4$  in Figure 12); the lower section extends from the tower base to the lower arm, and the other sections are terminated by the tower arms, which are not included in the equivalent circuit of the tower. In Figure 12b, the corresponding electrical circuit is displayed. Each section is represented by the series of a uniform lossless TL and a lumped impedance. The characteristic impedance  $Z_{T_i}$  of section  $i = 1, \dots, (N_s - 1)$  is set equal to  $220 \Omega$ , while  $Z_{T_{N_s}} = 150 \Omega$ . Interpretation of experimental results performed on a 62.8 m double-circuit tower for a power line with 500 kV rated voltage [55] showed that the propagation velocity of surges along the tower is very close to  $c_0$ . As a result, the model proposed by Ishii et al. adopts a propagation velocity  $c_T = c_0$ .

The damping impedance consists of the parallel of a resistor  $R_i$  (modeling attenuation along the tower), and an inductor  $L_i$  (influencing the shape of the traveling surges tail and not representing the value of the tower physical inductance). At low frequencies, i.e., at late times, the attenuation provided by the damping resistance is progressively reduced by the shunting function of the parallel inductor. These are computed as follows [59]:

$$R_i = \frac{-2Z_{T_i} \ln(\sqrt{\gamma})}{\sum_{m=1}^{N_s-1} h_m} h_i \text{ for } i = 1, \dots, (N_s - 1) \tag{33a}$$

$$R_{N_s} = -2Z_{T_{N_s}} \ln(\sqrt{\gamma}) \tag{33b}$$

$$L_i = R_i \frac{2h_T}{c_T} \text{ for } i = 1, \dots, N_s . \tag{33c}$$

In (33c),  $c_T = c_0$  is the surge propagation velocity, and  $\gamma = 0.8$  is the attenuation coefficient. Although the choice of the model parameters is related to experimental activity

on a specific HV double-circuit tower, the authors claim that they might be still used for other tall HV towers with similar structure.

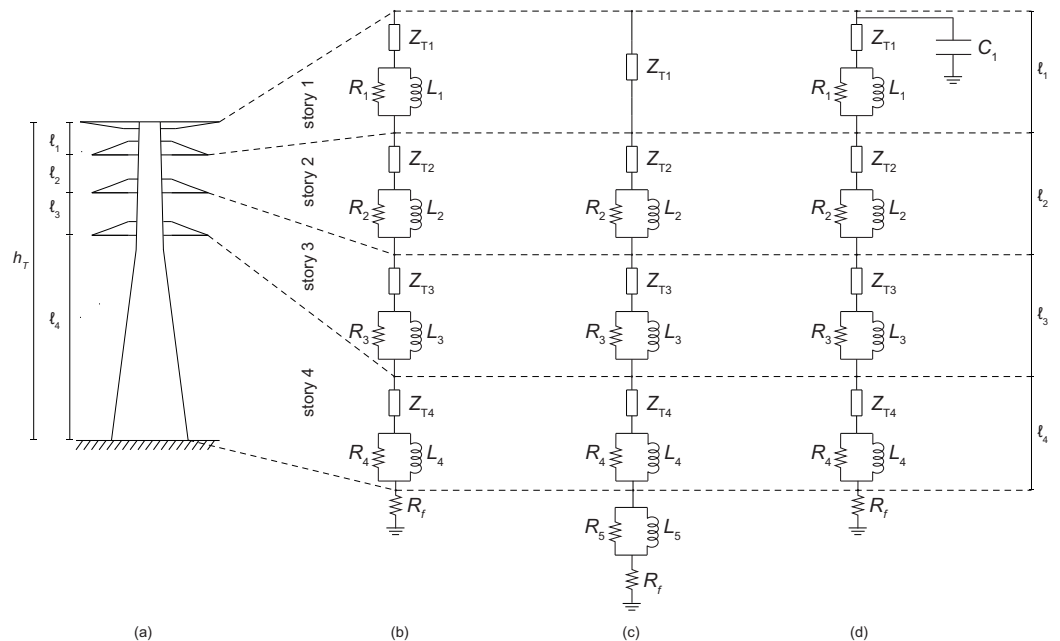


**Figure 12.** Sketch of a generic double-circuit tower taken as a reference (a), and three equivalent circuits according to different multistory models; (b) Ishii et al. model [55], (c) Baba et al. model [56], (d) Hashimoto et al. model [57].

The multistory model, as proposed in [55], and the simple TL approach (with surge propagation speed  $c_T \simeq 0.7c_0$ , and characteristic impedance  $Z_T = 100 \Omega$ ) were implemented in [86] to compare computed results against experimental data from backflashover events for a 77 kV line with height equal to 37.7 m. Since the results obtained by the multistory model were not satisfactory, the authors suggest not to include the lumped  $R - L$  circuits (originally derived for a 500 kV tower) when implementing this approach to simulate sensibly shorter towers for networks at lower rated voltage.

#### 4.3.2. Baba et al. Model

Later studies on TL-type circuits for tower modeling have been performed by Baba et al. [56], who initially investigated the influence of the different elements of the tower on its overall surge impedance [87] (intended as the ratio of the voltage peak measured at the tower top over the current at the same time instant). The corresponding surge impedances are computed for a reference four-leg structure over a PEC surface, with height equal to 120 m; each leg is connected to the plane by a  $40 \Omega$  resistor (corresponding to an overall footing resistance  $R_f = 10 \Omega$ , if no interaction is assumed). Results are obtained by the electromagnetic code NEC, implementing the method of moments.

While the bracings horizontal elements result in negligible differences in the voltage responses evaluated at the tower top (for a step current excitation), the diagonal elements and arms reduce the voltage peak value, the arms contribution being represented by additional capacitances from the arms towards the ground. Furthermore, the total traveling time of surges from the tower top to the base is increased if the bracings are included in the numerical simulation. Larger radii of the tower main legs are found to reduce the surge impedance.

For the aforementioned configuration under test, values of the characteristic impedances, damping resistors and inductors are given to represent the tower by means of a multistory model [88,89]. However, to more satisfactorily reproduce the decaying trend of the reference voltages computed at the insulator strings through the electromagnetic code,

an additional  $R - L$  circuit is added in series to the lower story (depicted in Figure 12c); no lumped circuit is included in the modeling of the tower's uppermost section.

The proposed  $Z_{T_i}$  (which is claimed to be suitable for simulation of double-circuit towers) was initially employed to derive the values of resistors  $R_2$  and  $R_3$  so as to minimize reflections at the nodes of the tower equivalent circuit (i.e.,  $R_i = Z_{T_i} - Z_{T_{i+1}}$  with  $i = 2, 3$ ). The values of  $R_4$  and  $R_5$  derive from a trial-and-error process. Time constants of the parallel circuits  $R_4 - L_4$  and  $R_5 - L_5$  are chosen to reproduce the observed trends of the voltage tails across the insulators, and the transient impedance of the grounding system, respectively [56]. Indeed, the series of the footing impedance  $R_f$  and  $R_5 - L_5$  results, in the time domain, in an increased transient grounding resistance at early-time.

#### 4.3.3. Hashimoto et al. Model

Noda ([60], in Japanese) proposed a modified multistory model for a 77 m-tall tower; a single  $R - L$  circuit is connected at the tower TL equivalent, namely, to the lowest story. An additional capacitance  $C_T$  connects the tower top to the ground, and controlled voltage sources are introduced at the phases for correction of the insulator voltages. Time domain waveforms computed by Noda were used by Hashimoto et al. [57] to propose the modified multistory model in Figure 12d for the same 77 m tower.

In particular, the self and mutual characteristic impedances of the shield wires and phase conductors are computed with the EMTP program, and an approximation for their coupling coefficients is obtained. From known current distribution between tower and shield wire [60], the characteristic impedance associated to the first story  $Z_{T_1}$  in Figure 12d is derived by means of a current divider, referring to currents at  $t^* = 2h_T/c_T$  (in this model, the value  $c_T = 276 \text{ m}/\mu\text{s}$ —first derived by Noda from recorded voltage waveforms—is adopted for the surge propagation speed):

$$Z_G I_{t^*,G} = Z_{T_1} I_{t^*,T}, \quad (34)$$

where  $I_{t^*,T}$  is the known current flowing along the tower at  $t^*$ ;  $I_{t^*,G}$  accounts for the sum of currents flowing along the shield wire at  $t^*$ , split into opposite directions at the tower top;  $Z_G$  denotes the halved characteristic impedance of the ground wire.  $Z_{T_i}$  for  $i > 1$  is derived from the known values of the insulator peak voltages [60]. In particular, if  $V_{\text{ins},i}$  denotes the voltage across the insulator of phase  $i$  ( $i = 1, 2, 3$  for the uppermost, central, and lower phase, respectively) and  $\kappa_i$  is the coupling coefficient between the shield wire and phase conductor  $i$ ,  $Z_{T_i}$  is found as follows

$$Z_{T_{i+1}} = \frac{V_{\text{ins},i} + \kappa_i (Z_{T_1} I_T)}{I_T}. \quad (35)$$

The values of  $R_i$  ( $i = 3, \dots, 1$ ) in Figure 12d are chosen to avoid reflections between adjacent stories (considering the TL representative of the fourth story to be infinite, or to be closed on a matched load); the values of  $L_i$  are computed in order for the time constant of the  $R_i - L_i$  circuit to match the double of the tower traveling time  $\tau = h_T/c_T$ :

$$R_i = Z_{T_i} - Z_{T_{i+1}} \quad (36a)$$

$$L_i = 2\tau R_i. \quad (36b)$$

The known steady-state currents flowing along the tower and the shield wire (towards the right and left sides of the tower) allow to size the current divider consisting of  $Z_G$  and  $R_F$  (hence, to derive a suitable value of the steady-state impedance of the tower  $R_F$ ). Values of  $R_4$  and  $L_4$  are associated with the estimated reflection coefficient at the tower base and fitting of available current data in the time domain.

The value of  $C_T$  is chosen in order for the model to reproduce the known time necessary for the upper-phase insulator voltage to reduce to the 63% of its peak value.

Although results computed by Hashimoto et al. for the tower under study were in accordance with the ones simulated by Noda by an FDTD method, some remarks on the adopted assumptions of the method are needed. The choice of  $t^*$  to derive  $Z_{T_i}$  by a current divider is arbitrary. Approximations are introduced in the evaluation of phase conductors' voltages and coupling coefficient that might affect the accuracy of the results. Indeed, the availability of data for currents and insulator voltages is required to adjust the model parameters and derive the needed impedances; hence, the model cannot be implemented unless experimental (or FDTD simulated in the time domain) data are available.

#### 4.3.4. Motoyama et al. Model

Initial experimental investigations by Motoyama et al. [58] involved 59.4 m-high towers of a 2.15 km double-circuit line with 245 kV rated voltage and a single shield wire connected at the tower peak. One of the towers was provided with sensors and optical fiber connections in order to measure natural and triggered lightning currents, splitting of the current between the tower and the shield wire, and voltages across the insulator strings. A multistory model like the one displayed in Figure 12b was adopted with values in Table 4; however, new constant-valued characteristic impedances  $Z_{T_i} = 120 \Omega$  (for  $i = 1, \dots, 4$ , found empirically, and different from the ones originally proposed by Ishii et al.) were observed to better reproduce measured currents and voltages with  $\gamma = 0.8$ .

**Table 4.** Parameters required by the main multistory models presented in Section 4.3.

Model	Story 1	Story 2	Story 3	Story 4
Ishii et al. [55]	$Z_{T_1} = 220 \Omega$ $\gamma = 0.8$	$Z_{T_2} = 220 \Omega$ $\gamma = 0.8$	$Z_{T_3} = 220 \Omega$ $\gamma = 0.8$	$Z_{T_4} = 150 \Omega$ $\gamma = 0.8$
Baba et al. [56]	$Z_{T_1} = 200 \Omega$	$Z_{T_2} = 200 \Omega$ $R_2 = 20 \Omega, \tau_2 = \frac{2ht}{c_0}$ <sup>a</sup>	$Z_{T_3} = 180 \Omega$ $R_3 = 30 \Omega, \tau_3 = \frac{2ht}{c_0}$	$Z_{T_4} = 150 \Omega$ $R_4 = 25 \Omega, \tau_4 = \frac{4ht}{c_0}$ $R_5 = 25 \Omega, \tau_5 = \frac{0.4ht}{c_0}$
Motoyama et al. [58]	$Z_{T_1} = 120 \Omega$ $\gamma = 0.8$	$Z_{T_2} = 120 \Omega$ $\gamma = 0.8$	$Z_{T_3} = 120 \Omega$ $\gamma = 0.8$	$Z_{T_4} = 120 \Omega$ $\gamma = 0.8$
Yamada et al. [59]	$Z_{T_1} = 120 \Omega$ $\gamma = 0.7$	$Z_{T_2} = 120 \Omega$ $\gamma = 0.7$	$Z_{T_3} = 120 \Omega$ $\gamma = 0.7$	$Z_{T_4} = 120 \Omega$ $\gamma = 0.7$

<sup>a</sup> where the value of the lumped inductance is found as  $L_i = R_i \tau_i$ .

In [74], further research was devoted to develop a general approach and prove that the direction of the injected current at the tower top holds an influence on the tower surge impedance (defined as the ratio of the time dependent voltage at the tower top and the value of the injected step current). In particular, two currents start propagating at time  $t = 0$  from the tower top: one flows vertically along the tower (due to the migration of negative charges), while a return-stroke current (produced by the migration of positive charges) flows upward in the lightning channel, with incline  $\varphi$  with respect to the horizontal plane. Indeed, the derived expression of the electric field in the time domain accounts for the contributions of the magnetic vector potential and of the scalar electric potential, which are produced by the return-stroke current in the injection channel and by the current flowing along the tower.

The tower is reduced to an equivalent cylinder with radius  $r_e$  equal to an algebraic mean of the tower arms lengths (including possible arms supporting shield conductors of the specific tower design).

The PEC plane approximation is adopted for the tower base, uniform currents are assumed for the injection channel and the tower path, and constant propagation velocity  $c_r$  and  $-c_T$  are adopted for the charges flowing along the return-stroke and the tower axis, respectively. These latter quantities are deduced from experimental activity on reduced and full-scale towers with heights ranging between 3 m and 120.5 m (relation  $c_T < c_r$  holds for all the investigated cases,  $c_r \simeq 300 \text{ m}/\mu\text{s}$ ).

Denoting with  $E_{r,z}$  and  $E_{t,z}$  the component of the electric field in the  $z$  direction on the external surface of the equivalent cylinder, due to the return-stroke current and the current along the tower, and adopting the following definition for the tower top voltage

$$V_T(t) = - \int_0^{h_T} E_z(t) dz = - \int_0^{h_T} (E_{t,z}(t) + E_{r,z}(t)) dz, \tag{37}$$

the transient surge impedance  $Z_{TV}$  when the step current is injected in a vertical direction ( $\varphi = \pi/2$  in Figure 13) is given by:

$$Z_{TV} = \frac{30}{\hat{c}_r} \left\{ \ln \left[ \frac{d + \sqrt{d^2 + r_e^2}}{r_e} \right] - (1 - \hat{c}_r^2) \ln \left[ \frac{c_r t + d + \sqrt{(c_r t + d)^2 + (1 - \hat{c}_r^2) r_e^2}}{c_r t + \sqrt{(c_r t)^2 + (1 - \hat{c}_r^2) r_e^2}} \right] \right\} + \frac{30}{\hat{c}_T} \left\{ \ln \left[ \frac{d + \sqrt{d^2 + r_e^2}}{r_e} \right] + (1 - \hat{c}_T^2) \ln \left[ \frac{c_T t - d + \sqrt{(c_T t - d)^2 + (1 - \hat{c}_T^2) r_e^2}}{c_T t + \sqrt{(c_T t)^2 + (1 - \hat{c}_T^2) r_e^2}} \right] \right\} \tag{38}$$

for  $\frac{r_e}{c_0} \leq t < t^*$

with

$$\hat{c}_T = c_T / c_0, \hat{c}_r = c_r / c_0 \tag{39a}$$

$$t^* = \sqrt{(2h_T)^2 + r_e^2} / c_0 \tag{39b}$$

$$d = \sqrt{(c_0 t)^2 - r_e^2}. \tag{39c}$$

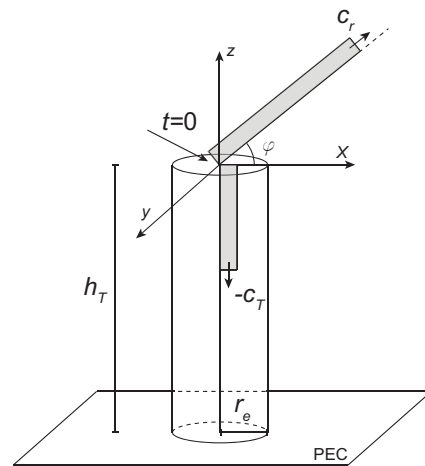


**Figure 13.** Reference configuration for the derivation of the tower surge impedance adopted by Motoyama et al. [74], considering the influence of the direction of the return-stroke current, and of different velocities of charges in the return-stroke channel and along the tower (represented by an equivalent cylinder).

The expression of  $Z_{TH}$  for horizontal injection ( $\varphi = 0$  in Figure 13) is

$$\begin{aligned}
Z_{TH} = & \frac{30}{\hat{c}_r} \left\{ \ln \left[ \frac{c_0 t}{r_e} \right] + \ln \left[ \frac{c_r t + \sqrt{(c_r t)^2 + (1 - \hat{c}_r^2) r_e^2}}{c_r t + \sqrt{(c_r t)^2 + (1 - \hat{c}_r^2) (c_0 t)^2}} \right] \right\} + \\
& + \frac{30}{\hat{c}_T} \left\{ \ln \left[ \frac{d + \sqrt{d^2 + r_e^2}}{r_e} \right] + (1 - \hat{c}_T^2) \ln \left[ \frac{c_T t - d + \sqrt{(c_T t - d)^2 + (1 - \hat{c}_T^2) r_e^2}}{c_T t + \sqrt{(c_T t)^2 + (1 - \hat{c}_T^2) r_e^2}} \right] \right\} \\
& \text{for } \frac{r_e}{c_0} \leq t < t^* \quad (40)
\end{aligned}$$

In the time interval  $0 \leq t < r_e/c_0$ , a null impedance is assumed to account for the time required for the field to propagate from the cylinder axis to its external surface. At times  $t > t^*$ ,  $Z_{TH}$  and  $Z_{TV}$  are approximated by the value attained at  $t = t^*$ , neglecting subsequent reflections. Furthermore, expressions (38) and (40) are limited to the case of step current excitation; the tower surge impedance under different excitations should be derived through integral relations. However, the application of this approach led to a good agreement with measured voltages on a test UHV tower.

Experimental activity was performed over a double-circuit tower (rated voltage 500 kV, height 89.5 m), without shield wires and phase conductors. A step current was injected at the tower top through a suitable injection wire, to investigate the influence of its incline with respect to the ground on the computed value of the tower surge impedance (ratio of the maximum voltage at the tower peak over the current injected at the same time instant) and surge response (voltage at the top as a function of time over the peak of the injected current) [90]. A significant influence of the direction of current injection was observed; in particular, the voltage at the tower top is larger as the angle of the current injection wire is increased from  $0^\circ$  (horizontal position) up to  $30^\circ$ . The propagation velocity along the line has been estimated as approximately equal to  $c_T \simeq 0.9c_0$ , not depending on the direction of current injection. FDTD simulations were performed to account for larger injection angles (namely,  $30^\circ < \varphi < 90^\circ$  in Figure 13), and reproduce the approximate vertical direction of impinging lightning currents. An average increasing trend of the voltages' peak value was found (approximately 30% larger than computed peak values for the horizontal injection case).

#### 4.4. Non-Uniform Transmission Lines

Models presented in Sections 4.2.3 and 4.3, which were classified as multiconductor or multistory models, could also be intended as non-uniform TL models. In fact, by application of these approaches, the tower is partitioned into a limited number of sections, represented by equivalent TLs with potentially different (but constant) characteristic impedances.

Tower models here classified as actual non-uniform TL models (reviewed in the following section) define the characteristic impedance as a continuous function of the height above the ground.

##### 4.4.1. Gutierrez et al. Model

Gutierrez et al. developed a multiconductor model for the tower [53,54], accounting for the finite conductivity of the earth; indeed, a reference plane at zero potential is introduced at a complex depth  $h_c$  (defined in Section 4.2.3).

In particular, the value of the characteristic impedance at height  $h$  of the equivalent non-uniform TL is found from the known expression of the electric field in the polar direction  $\theta$  produced by a biconical antenna with the vertex  $O$  lying on the plane at complex depth. In the frequency domain, the characteristic impedance is computed as the ratio of the voltage at height  $h$  above the ground and the current flowing along the tower.

With reference to the configuration in Figure 14, the parallel vertical conductors are intended to approximate two legs of the tower. Parameters  $r_i$  and  $d_{ij}$  denote the leg radius

and the mutual distance between the axis of leg  $i$  and  $j$ , respectively. The expression of the progressive-dependent mutual characteristic impedance is given by:

$$Z_{T,ij} = \sqrt{\frac{\mu_0}{\epsilon_0}} \frac{e^{-j\beta(R_{ij}-R)}}{2\pi} \ln \left[ \cot \left( \frac{\theta_{ij}}{2} \right) \right] \tag{41}$$

with

$$\cot \left( \frac{\theta_{ij}}{2} \right) = \left[ \frac{\sqrt{h^2 + d_{ij}^2} + h}{d_{ij}} \right] \left[ \frac{\sqrt{(h + h_c)^2 + d_{ij}^2} + h + h_c}{\sqrt{h^2 + d_{ij}^2} + h} \right]. \tag{42}$$

In (41) and (42),  $\theta_{ij}$  is the complex angle with vertex  $O$ —due to the reference plane at complex depth  $h_c$ —between the axis of the vertical conductor  $i$  and the observation point on the axis of conductor  $j$ ;  $R_{ij}$  and  $R$  denote the distance between the vertex  $O$  and the observation point on conductor  $j$  axis and on the external surface of conductor  $i$ , respectively, at height  $h$  above the ground. Equation (41) allows to compute mutual terms of the matrix of characteristic impedances of the multiconductor system consisting of the four tower legs; the self-term may be obtained with  $i = j$ ,  $d_{ij} = r_i$ , and  $R_{ij} = R$  ( $\theta_{ii}$  denoting the half-angle of aperture of the cone displayed in Figure 14).

Algebraic manipulation of (41) and (42) allows to identify the two following contributions,  $Z_{ij}^G$  and  $Z_{ij}^E$

$$Z_{T,ij} = Z_{ij}^G + Z_{ij}^E \tag{43}$$

with

$$Z_{T,ij}^G = \sqrt{\frac{\mu_0}{\epsilon_0}} \frac{e^{-j\beta(R_{ij}-R)}}{2\pi} \ln \left[ \frac{\sqrt{h^2 + d_{ij}^2} + h}{d_{ij}} \right] \tag{44a}$$

$$Z_{T,ij}^E = \sqrt{\frac{\mu_0}{\epsilon_0}} \frac{e^{-j\beta(R_{ij}-R)}}{2\pi} \ln \left[ \frac{\sqrt{(h + h_c)^2 + d_{ij}^2} + h + h_c}{\sqrt{h^2 + d_{ij}^2} + h} \right]. \tag{44b}$$

In (44),  $Z_{ij}^G$  and  $Z_{ij}^E$  may be identified with the mutual (characteristic) geometric impedance and earth impedance between vertical conductors  $i$  and  $j$ , respectively. As for tower crossarms, each tower arm can be decomposed into a vertical and a horizontal TL with different lengths, depending on the arm incline with respect to the ground plane [53].

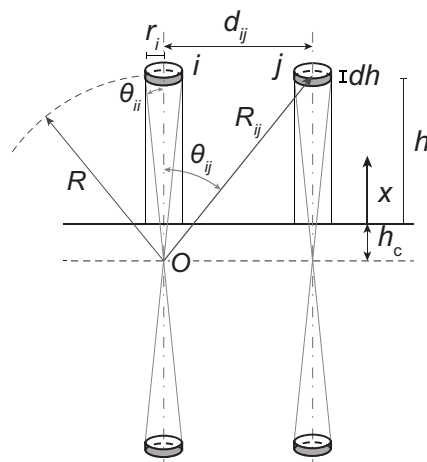


**Figure 14.** Reference quantities required by Gutierrez et al. approach to derive self and mutual characteristic impedances of the tower legs.



As for p.u.l. impedance  $\mathbf{Z}$  and admittance  $\mathbf{Y}$  matrices (for four conductors, i.e., the four legs of the tower), these are computed as follows:

$$\mathbf{Z} = j\frac{\omega}{c_0}\mathbf{Z}^G + j\frac{\omega}{c_0}\mathbf{Z}^E + \mathbf{Z}^C \quad (45a)$$

$$\mathbf{Y} = j\frac{\omega}{c_0}\left(\mathbf{Z}^G\right)^{-1}. \quad (45b)$$

In (45b), elements of the matrices  $\mathbf{Z}^G$  and  $\mathbf{Z}^E$  correspond to (44a) and (44b), respectively;  $\mathbf{Z}^C$  is a diagonal matrix accounting for the conductor p.u.l. internal impedance, with diagonal elements given by:

$$Z_{ii}^C = R_{ii}^C + j\omega L_{ii}^C = \sqrt{j\omega\mu\rho}/(2\pi r_i), \quad (46)$$

where  $\mu$  and  $\rho$  denote the magnetic permeability and electrical resistivity of the leg conductor material, and the second equivalence is derived assuming  $\rho^{-1} \gg \omega\epsilon_0$  and  $r_i > 2\delta$  ( $\delta$  being the skin depth in the conductor at angular frequency  $\omega$ ) [91]. Satisfactory accuracy is reached when reproducing the voltage response of a HV tower (62.8 m high) to an injected current measured by Ishii et al. [55]; only around 2% difference is obtained for the peak value of the computed voltage at the tower top with respect to measurements.

The proposed formulation is based on the validity of two relevant assumptions. The excited range of frequency should be such that the finite conductivity of the ground may be still accounted for by the complex depth approach [85]; in other words, the ground can be considered as a good conductor  $\sigma_g \gg \omega\epsilon_g$  (where  $\epsilon_g$  is the ground electric permittivity). If the truss shows a large aspect ratio (i.e., for  $h \gg r_i$ ), the field produced by the current flowing along the tower can be treated as a spherical wave; as a result, the known expression of the TEM field emitted by a biconical antenna (with height-dependent half-angle, and accounting for  $h_c$ ) is used to approximate the electric field and is integrated to derive the voltage along the conductors. The matrix of p.u.l. capacitances does not account for the lossy ground; furthermore, a reversed, approximated procedure is implemented to compute the p.u.l. impedance associated with the geometrical inductance and ground. Indeed, these are *not* derived by electromagnetic field theory and employed to compute the tower characteristic impedance; vice versa, they are derived starting from the characteristic impedance, assuming the propagation constant to be equal to that of vacuum as a first approximation.

Variations of the same approach have been recently proposed in the literature by Guo et al. [92].

#### 4.4.2. Saied et al. Model

The tower is modeled as a non-uniform lossless TL; indeed, its surge impedance is expressed as a function of  $x$ .

Initially, the characteristic impedance was expressed by a function of the distance of the observation point from the tower base [47]. In particular, at distance  $x$  from the ground, the characteristic impedance is computed as a power function of  $x$  (The right-hand sides of (47)–(50) are expressed in Ohm, when  $x$  is expressed in meters):

$$Z_T(x) = Z_0x^\alpha, \quad (47)$$

where  $Z_0$  is a constant to be determined. The choice of this specific function was aimed at obtaining an analytical, closed-form expression of the travelling voltage waves by substitution of (47) in the second-order differential equation written in the line voltages for TL applications in the Laplace domain. Hence, the expression of the height-dependent characteristic impedance  $Z_{TM}(x)$  in (48) proposed by Menemenlis et al. [68] (originally developed to simulate the electrical behavior of a tower with height equal to 75 m)

$$Z_{TM}(x) = 50 + 35\sqrt{x} \quad (48)$$

is approximated by a power law expression of the type (47) with  $Z_0 = 64.04$  and  $\alpha = 0.39$ .

It should be noted that expression (48) does not depend on the tower geometrical features.  $Z_0$  and  $\alpha$  can be chosen to approximate (e.g., by the least squares method) other given expressions for  $Z_T(x)$  (as the one in (48)), or to match finite values of characteristic impedances of the sections under analysis (assumed arbitrarily, or derived empirically).

An alternative approach (introduced in [47], and implemented in [48]) was used to simulate non-uniform lines, starting from a given characteristic impedance (e.g., the one expressed by (48)), and deriving the corresponding tower model in the form of an exponential TL. The generic expression of the characteristic impedance  $Z_T(x')$  of the equivalent TL is:

$$Z_T(x') = Z_0 e^{kx'} \tag{49}$$

The tower is modeled as the cascade of a finite number of TLs with characteristic impedance  $Z_{T_i}(x')$ . With reference to Figure 15, if (48) is adopted and section  $i$  extends from  $x' = x'_{i-1}$  to  $x'_i > x'_{i-1}$  (with  $\ell_i = x'_i - x'_{i-1}$ ),  $Z_{0_i}$  and  $k_i$  are computed as:

$$Z_{0_i} = Z_{T_M}(h_T - x'_{i-1}) \tag{50a}$$

$$k_i = \frac{1}{\ell_i} \ln \left[ \frac{Z_{T_M}(h_T - x'_i)}{Z_{T_M}(h_T - x'_{i-1})} \right] \tag{50b}$$

In (50),  $x = h_T - x'$  has been considered to account for the different coordinate system adopted by the equivalent exponential TL model (in Figure 15). Hence, for the progressive-dependent characteristic impedance of section  $i$  the following holds:

$$Z_{T_i}(x') = Z_{0_i} e^{k_i(x' - x'_{i-1})} \text{ for } x'_{i-1} \leq x' \leq x'_i \tag{51}$$

Surge propagation velocity is set equal to  $c_0$ .

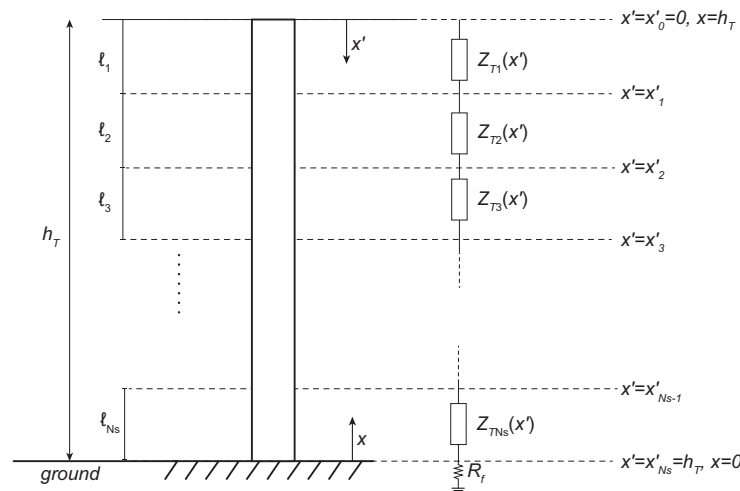


Figure 15. Non-uniform transmission line model of the tower according to Saied, Oufi et al. [47,48].

Although the tower is still divided into sections, each section is represented by an exponential TL with a characteristic impedance, which varies continuously with the progressive  $x'$ ; the following closed-form expression of the input impedance  $Z_{in}$  seen at the tower top is found in the  $s$  domain [48]:

$$Z_{in}(s) = \frac{V(s)}{I(s)} = sL_0 \frac{D_1(s)e^{\lambda_2 h_T} - D_2(s)e^{\lambda_1 h_T}}{\lambda_2 D_2(s)e^{\lambda_1 h_T} - \lambda_1 D_1(s)e^{\lambda_2 h_T}} \tag{52}$$

where  $V(s)$  and  $I(s)$  are the voltage and the injected current at the tower top, and functions  $D_1(s)$ ,  $D_2(s)$  are given by:

$$D_1(s) = sL_0e^{kh_T} + \lambda_2 Z_f(s), \quad D_2(s) = sL_0e^{kh_T} + \lambda_1 Z_f(s) \quad (53)$$

with

$$\lambda_1 = \frac{k}{2} + \sqrt{\frac{k^2}{4} + \frac{s^2}{c_0^2}}, \quad \lambda_2 = \frac{k}{2} - \sqrt{\frac{k^2}{4} + \frac{s^2}{c_0^2}}. \quad (54)$$

In (53),  $Z_f(s)$  denotes the tower footing impedance, i.e., the load connected at the termination of the equivalent TL; in (53) and (54),  $k$  is computed by (50b) when the tower is considered as a single section

$$k = \frac{1}{h_T} \ln \left[ \frac{Z_{T_M}(0)}{Z_{T_M}(h_T)} \right], \quad (55)$$

and  $L_0 = Z_T(0)/c_0 \simeq Z_{T_M}(h_T)/c_0$  (the second equivalence being valid only when (48) is adopted to approximate the characteristic impedance).

Results for a 75 m tower are presented in [48]; the exponential line approach is implemented starting from the expression of the characteristic impedance given by Mennenlis et al. (48). It is shown that a small number of TLs (the case of three cascaded TLs is presented) leads to acceptable results, and there is no significant discrepancy in computed voltages and transient surge impedances when modeling the tower through a larger number of cascaded TLs. Nevertheless, the exponential line model represents a methodology to assess the propagation along the tower; indeed, the function of  $x$  chosen to approximate the line characteristic impedance is expected to affect results predominantly.

#### 4.4.3. Almeida and Correia De Barros Model

Almeida and Correia de Barros proposed a non-uniform TL model of the tower. The line is discretized in segments (results are presented for 314 sections in [49]) to be represented by uniform TLs; the characteristic impedance  $Z_{T_i}$  of the  $i$ th TL is computed from  $Z_{T_{i-1}}$  of the adjacent one:

$$Z_{T_i} = \kappa Z_{T_{i-1}}. \quad (56)$$

The value of the adimensional constant  $\kappa$  is computed according to the degree of discretization adopted for the model. If the tower is divided into  $N_s$  sections and values are assigned to the TLs characteristic impedances associated to the uppermost and base sections ( $Z_{T_1}$  and  $Z_{T_{N_s}}$ , respectively), the value of  $\kappa$  is found as  $\kappa = \sqrt[N_s]{Z_{T_{N_s}}/Z_{T_1}}$ .

A second, more general, approach is presented in [50], addressing the problem in the time domain, solving the equations for the propagation of voltage and current waves by means of an FDTD method. The finite-difference approximation of the tower, i.e., its discretization into small  $\Delta x$ , allows to take into account the variation in the characteristic impedance with the  $x$  direction. If the space discretization is sufficiently fine, an additional resistance may be added in the Pi-equivalent circuit of the TL to account for longitudinal losses in the space step  $\Delta x$ ; however, the approach incorporates only an  $x$ -dependent resistance  $R(x)$ , neglecting any frequency dependency of the p.u.l. losses along the tower:

$$R(x) = -2 \frac{\log \sqrt{\gamma}}{h_T} Z_T(x); \quad (57)$$

expression (57) is of the same type as (33a), with  $\gamma = 0.8$ . In a similar fashion as the approach presented in Section 4.4.2, this model represents a tool to be implemented for known (or assumed) values of the characteristic impedances associated with the uppermost and the lowest sections of the tower. Hence, the reliability of the computed results depends on the approach itself, along with the choice of  $Z_{T_1}$  and  $Z_{T_{N_s}}$ . Furthermore, results computed by means of the proposed approach, when simulating Ishii et al. experiment [55], are not in

complete agreement with the measured data (e.g., when identifying the insulator which undergoes the largest electrical stress).

#### 4.4.4. Other Models

Different HV towers were simulated by means of equivalent multistory models derived from Ishii et al. Variations in the values of the characteristic impedances of the tower sections and attenuation constants were found to be more suitable to reproduce results from experimental activities performed on different structures.

Yamada et al. [59] performed experimental tests (similar to those conducted by Ishii et al. [55]) on an UHV double-circuit line of height approximately equal to 140 m. A multistory model, of the same type as that proposed by Ishii et al., is used to reproduce the electrical behavior of the tower. However, new values for the attenuation coefficient and characteristic impedances of the tower sections were proposed in order for the simulated results to be in satisfactory agreement with data measured across the insulators with a ramp current injected at the tower top (rise time  $\sim 1 \mu\text{s}$ ). In particular, with reference to the tower displayed in Figure 12 and the equivalent circuit in Figure 12b,  $Z_{T_i} = 120 \Omega$  for  $i = 1, \dots, 4$ , while  $\gamma = 0.7$  was assumed. The surge propagation velocity is equal to  $c_0$ .

The same value for the characteristic impedances of the multistory model of a double-circuit tower (of height 59.4 m, rated voltage 245 kV) was employed by Motoyama et al. [58]; however, the attenuation coefficient  $\gamma$  was set to 0.8, in accordance with Ishii et al. The experimental results were obtained by measurement of relevant voltages across the tower insulators for 10 lightning events, i.e., for lightning currents (natural or rocket-triggered) striking a rod installed on the top of the observed tower of the line under test. The simulated results differ from the measured ones in the peak values of the predicted voltages. Table 5 displays values of characteristic impedances, resistors and inductors computed for tower (a) in Figure 16 by the most common multistory models (according to expressions in Table 4).

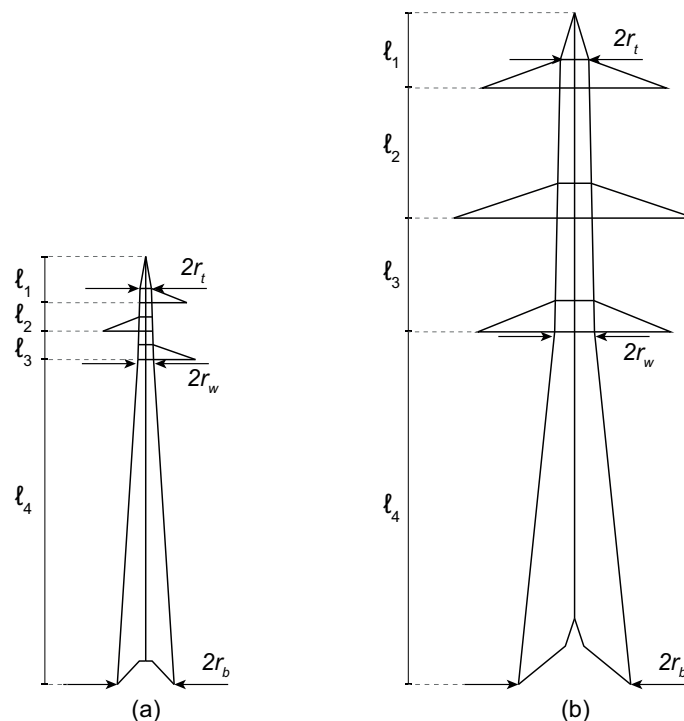


**Figure 16.** Typical towers for HV overhead transmission lines. (a) Rated voltage 132 kV; (b) Rated voltage 380 kV.

Yamanaka et al. [31] recently compared results obtained by an FDTD code and those computed through a lossless TL approximation for a 500 kV double-circuit tower (76 m high) over a PEC plane. The lossless TL approach underestimated rise times and decay

times of the insulator voltages when a step current was injected at the top. Furthermore, FDTD simulations resulted in larger voltages across the upper insulators; on the contrary, these were found to occur at the lowest insulators by computations through the equivalent TL circuit (similar results were found in [50]). These differences are likely ascribed to the non-TEM modes, which are not accounted for by the lossless TL model adopted for the tower [31], and to the time required for the formation of the TEM mode itself. An alternative approach was proposed in the  $s$  domain [31], allowing to predict a logarithmically increasing voltage at the tower top under a step-current excitation; this is achieved by dividing the TL equivalent to the tower into multiple sections, with the same characteristic impedance, defined in the Laplace domain as:

$$Z_T(s) = Z_0 \frac{1}{1 + \tau_T s}, \quad (58)$$

with  $\tau_T = h_T/c_0$ . The new characteristic impedance (58) converges to the value associated to the TEM mode propagation with a first-order delay under a step current excitation. Additionally, the model defines step-current responses of traveling voltage waves, accounting for their distortion and attenuation. However, these quantities depend on time constants and parameters derived so as to reproduce voltages across the insulators from available FDTD simulations. The peak values of the voltages across the insulators, with tower heights ranging between 39.5 m and 86 m, obtained by the developed approach result in satisfactory agreement with those given by the FDTD code [31]. Further features and applications of the model may be found in [93,94].

**Table 5.** Typical values of characteristic impedances and lumped elements for the reference tower (a) in Figure 16 according to multistory models presented in Section 4.3.

Model	Story 1 $\ell_1 = 3.25$ m	Story 2 $\ell_2 = 2$ m	Story 3 $\ell_3 = 2$ m	Story 4 $\ell_4 = 22.95$ m
Ishii et al. [55]	$Z_{T_1} = 220 \Omega$ $R_1 = 22.0 \Omega$ $L_1 = 4.4 \mu\text{H}$	$Z_{T_2} = 220 \Omega$ $R_2 = 13.5 \Omega$ $L_2 = 2.7 \mu\text{H}$	$Z_{T_3} = 220 \Omega$ $R_3 = 13.5 \Omega$ $L_3 = 2.7 \mu\text{H}$	$Z_{T_4} = 150 \Omega$ $R_4 = 33.5 \Omega$ $L_4 = 6.7 \mu\text{H}$
Baba et al. [56]	$Z_{T_1} = 200 \Omega$	$Z_{T_2} = 200 \Omega$ $R_2 = 20 \Omega$ $L_2 = 4.0 \mu\text{H}$	$Z_{T_3} = 180 \Omega$ $R_3 = 30 \Omega$ $L_3 = 6.0 \mu\text{H}$	$Z_{T_4} = 150 \Omega$ $R_4 = 25 \Omega$ $L_4 = 10.1 \mu\text{H}$ $R_5 = 25 \Omega$ $L_5 = 0.8 \mu\text{H}$
Motoyama et al. [58]	$Z_{T_1} = 120 \Omega$ $R_1 = 12.0 \Omega$ $L_1 = 2.4 \mu\text{H}$	$Z_{T_2} = 120 \Omega$ $R_2 = 7.4 \Omega$ $L_2 = 1.5 \mu\text{H}$	$Z_{T_3} = 120 \Omega$ $R_3 = 7.4 \Omega$ $L_3 = 1.5 \mu\text{H}$	$Z_{T_4} = 120 \Omega$ $R_4 = 26.8 \Omega$ $L_4 = 5.4 \mu\text{H}$
Yamada et al. [59]	$Z_{T_1} = 120 \Omega$ $R_1 = 19.2 \Omega$ $L_1 = 3.9 \mu\text{H}$	$Z_{T_2} = 120 \Omega$ $R_2 = 11.8 \Omega$ $L_2 = 2.4 \mu\text{H}$	$Z_{T_3} = 120 \Omega$ $R_3 = 11.8 \Omega$ $L_3 = 2.4 \mu\text{H}$	$Z_{T_4} = 120 \Omega$ $R_4 = 42.8 \Omega$ $L_4 = 8.6 \mu\text{H}$

## 5. Evaluation of the Tower Model Influence on Transients Studies

In the following, the reviewed models are compared in terms of the input impedance seen at the tower top with different grounding conditions; additional voltages at the tower top  $v(t)$  in the time domain, computed when a first stroke or a subsequent stroke current [69] is injected, are discussed.

The two towers represented in Figure 16 are taken as a reference; in particular, towers in Figure 16a,b are referred to as tower (a) and (b), respectively. The corresponding geometrical features are listed in Table 6. Quantities  $r_b$ ,  $r_w$ , and  $r_t$  denote the radius of the circumferences that are inscribed in sections at the tower base, waist and top, respectively;  $r_a$  is the assumed equivalent radius of the tower crossarms;  $r_c$  is the radius adopted for the cylindrical conductors accounting for the tower legs (determined from dimensions of symmetrical L-shaped conductors with sides in the range of 12–18 cm, commonly used for the tower legs). Tower (a) (with height  $h_T = 30.2$  m) is representative of typical truss towers

for systems with 132–150 kV rated voltage, whereas tower (b) (with height  $h_T = 47.4$  m) is characteristic of double-circuit lines with 380–400 kV rated voltage. As for models that approximate the tower to a cylinder, the equivalent radius  $r_e$  has been computed as:

$$r_e = \frac{r_t h_t + r_w h_T + r_b h_b}{2h_T}, \tag{59}$$

with  $h_t = \ell_1 + \ell_2 + \ell_3$  and  $h_b = \ell_4$ . Indeed, the equivalent radius is not distinctively defined in the literature, although  $r_e$  noticeably affects the value of the characteristic impedance; as an example, Figure 17 shows  $Z_T$ , derived for tower (a) by the revised Jordan approach in Section 4.1.1, as a function of the adopted  $r_e$ . If  $r_e$  is chosen between the radius at the uppermost section and the one at the base of the tower, a wide range of variability is expected for the corresponding  $Z_T$ .

**Table 6.** Geometrical characteristics of the towers under analysis.

		Tower (a)	Tower (b)
$h_T$	[m]	30.2	47.4
$r_b$	[m]	2.0	3.95
$r_w$	[m]	0.55	1.4
$r_t$	[m]	0.4	2.0
$\ell_1$	[m]	3.25	5.3
$\ell_2$	[m]	2.0	9.2
$\ell_3$	[m]	2.0	8
$\ell_4$	[m]	22.95	24.9
$r_a$	[m]	0.25	0.5
$r_c$	[cm]	6.0	9.0

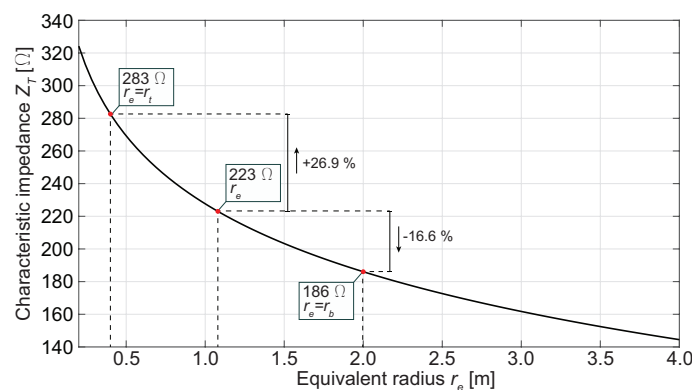


**Figure 17.** Variability in the characteristic impedance, computed for tower (a) in Figure 16 ( $h_T = 30.2$  m, rated voltage 132 kV) according to the revised Jordan formula in Section 4.1.1, with the choice of the tower equivalent radius  $r_e$ .

Two grounding systems, installed along Italian transmission lines, are considered. They are referred to as grounding types MT2 and MT4, their structure being sketched in Figure 18. Common practice in Italy consists of adopting the grounding system, which allows to obtain a grounding resistance  $R_{gr} \leq 20 \Omega$  (in the following, the symbol  $R_{gr}$  denotes the value attained by the grounding impedance  $Z_{gr}(f)$  at 50 Hz), when accounting for the specific soil properties. In Table 7, dimensions of the considered grounding systems, properties of the soil in which they are assumed to be buried, and corresponding values of  $R_{gr}$  are displayed.  $\rho_g$  and  $\epsilon_{r_{gr}}$  denote the soil electrical resistivity and relative permittivity;  $r_b$  is related to the dimensions of the towers at the base in Figure 16. The grounding structure, which is actually made of steel conductors with rectangular sections with dimensions  $4 \times 40$  mm, is modeled by means of equivalent cylindrical conductors with radius  $r_w$ ; the value of  $r_w$  (consistent with the one adopted in [95]) has been derived in order for the external surface of the adopted equivalent conductor to be equivalent to the actual one. Magnitude and argument of the input impedance offered by the MT2 and

MT4 grounding systems (computed by means of a hybrid code [13,96]) are displayed in Figure 19 as functions of frequency. It can be deduced that the DC value of the grounding impedance may be considered also for switching overvoltage studies (unless fast transients such as those ensuing from gas insulated substations have to be analysed); indeed, negligible differences are computed for the absolute value of the grounding impedances up to 10–100 kHz with respect to their low-frequency value (less than 1% at 100 kHz).

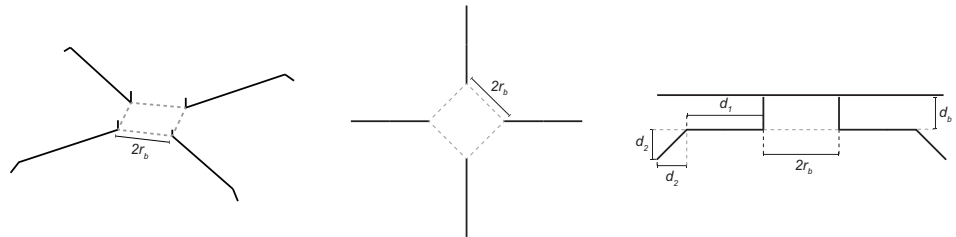


**Figure 18.** Structure of grounding system MT2 and MT4, commonly adopted along Italian transmission lines (not in scale).

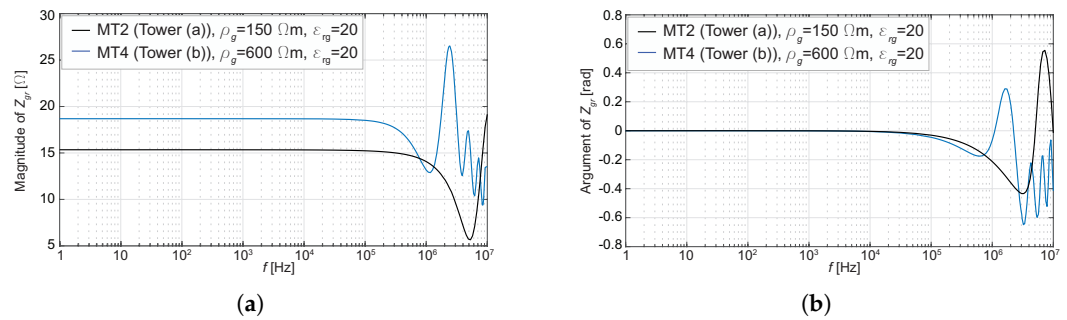


**Figure 19.** Grounding system impedance (magnitude and argument). (a) Magnitude. (b) Argument.

**Table 7.** Geometrical parameters and soil properties required for the characterization of the grounding systems under study.

Type	$d_1$ [m]	$d_2$ [m]	$d_b$ [m]	$r_b$ [m]	$r_w$ [mm]	$\rho_g$ [Ωm]	$\epsilon_{r_g}$ -	$R_{gr}$ [Ω]
MT2	1.0	1.0	0.8	2.0	14.0	150	20	15.3
MT4	12.0	1.0	1.0	3.95	14.0	600	20	18.7

The median negative first [97] and subsequent [98] stroke currents, depicted in Figure 20a, are injected at the tower top. Figure 21 is included to provide the reader with an example of the impact of higher frequency components of the injected currents (e.g., above 50 kHz); Figure 21a,b display the first and subsequent stroke currents used for results, and those obtained by means of the Inverse Fourier Transform (IFT) of their corresponding frequency spectrum, when it is truncated to its 50 kHz, 100 kHz, and 500 kHz component. Indeed, components at higher frequencies, despite their reduced magnitude, noticeably affect the front and peak values of the waveform in the time domain. If the spectra are to be truncated at 500 kHz, the computed time-to-peak value corresponds to 0.9 p.u. (per unit) and 0.7 p.u. of the one related to the actual first or subsequent stroke current, respectively; up to 100 kHz, the same quantities increase to 1.3 p.u. and 1.9 p.u.; if the cutoff frequency is chosen at 50 kHz, they increase to 1.7 p.u. and 3.1 p.u., respectively. A non-negligible effect might be observed also on the waveform peak values. The upper portion of the current spectrum should not be neglected, especially when the tower voltage is to be computed as the IFT of the product of the current with the tower input impedance (which may show resonances in the frequency range 1–10 MHz).

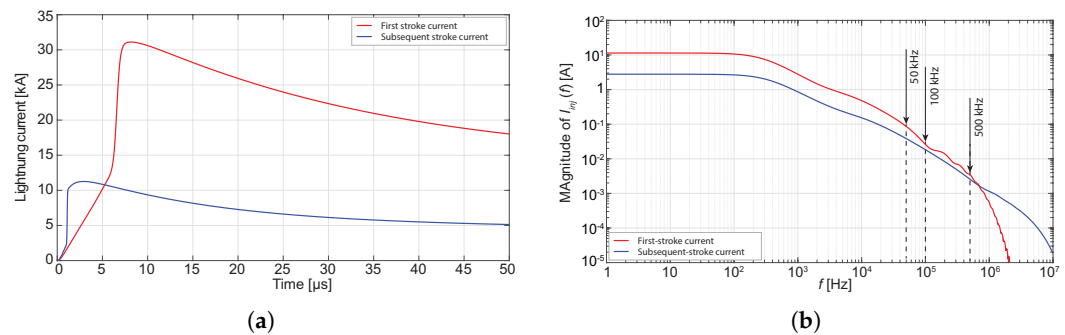


**Figure 20.** First and subsequent stroke currents injected at the top of the studied towers. (a) First [97] and subsequent [98] stroke currents in the time domain. (b) Frequency spectrum (magnitude) of the lightning currents in (a).

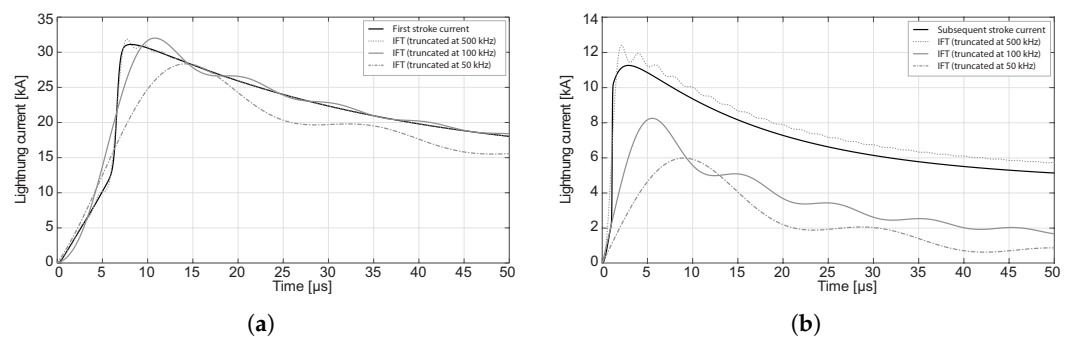


**Figure 21.** First and subsequent stroke currents obtained as the Inverse Fourier Transform of the frequency spectrum in Figure 20a, truncated at 500 kHz, 100 kHz, and 50 kHz. (a) First stroke current. (b) Subsequent stroke current.

Voltage  $v(t)$  for tower (a) over a PEC plane, computed by means of the reviewed models, are shown in Figures 22a and 23b, respectively (Gutierrez et al. model: tower partitioned in four sections. Almeida et al. model: tower partitioned in twenty sections). In Figure 23, the corresponding input impedances as seen at the tower top  $Z_{in}(f)$  are displayed. Multiple resonances may be observed in the  $Z_{in}$  by Hara et al. due to the additional modeling of the tower trussing and crossarms (i.e., horizontal TLs with open terminations). The wide range of variability in input impedances results in computed peak voltages ranging approximately between 0.3 and 0.8 MV, and from 0.8 to 1.8 MV, for the first and the subsequent stroke current, respectively. In Figure 23b, only  $Z_{in}$  by Gutierrez et al. shows a resistive-inductive behavior at low frequency; this is caused by the additional term associated with the legs' internal impedance.

Similar observations are valid for results computed for tower (b) over a PEC plane. The larger inductive impedance offered by  $Z_{in}$  of tower (b) in the range of 1–10<sup>5</sup> Hz (Figure 24) results in enhanced peak voltages at the tower top with the first stroke current. Peak voltages range between 0.5 MV and 1.3 MV with the first stroke current (Figure 25a), and between 0.8 MV and 1.8 MV with the subsequent stroke current (Figure 25b). As expected, periodical reflections from the tower base occur after longer time intervals (approximately equal to 0.32 μs), due to the increased height of tower (b). In Figure 25b, it should be noticed that voltages obtained by non-uniform TL models (listed in diagram Figure 2) display a different waveform; indeed, smaller reflections are caused by the mismatch between TL associated with adjacent sections of the tower.

Higher voltages are observed with the subsequent stroke current for both towers (Figures 22b and 25b) compared to the first stroke case (Figures 22a and 25a). This is due to the larger absolute value of the input impedances in the range 1–10 MHz, and to the non-negligible frequency components of the excitation in the same frequency range.



The influence of the soil resistivity  $\rho_g$  (considered by Ametani et al. model in Section 4.2.3, and Gutierrez et al. model in Section 4.4.1), and of the grounding systems is addressed in Figures 26–29. It can be observed that the inclusion of the grounding system limits the values of  $Z_{in}$  in the high-frequency range; up to 10 kHz,  $Z_{in}$  practically coincides with  $R_{gr}$  (Figures 26–28) and  $Z_{gr}$  (Figures 27–29). It is very important to highlight that the adoption of different models results in very different input impedances. Moreover, the tower geometry is of paramount importance and any generalization of drawn conclusions requires a careful check. The argument of the input impedance also deserves a word of caution: it may contribute to enhancing the differences between voltages ensuing from different models. An accurate analysis of Figures 26–30 clarifies the very large differences on the tower voltages appearing when different models are adopted. At 100 kHz, the absolute value of the computed input impedances is approximately in the range 17–29  $\Omega$  for tower (a), and 21–44  $\Omega$  for tower (b). Relevant differences are to be observed in the argument of  $Z_{in}$  too.

Eventually, Figure 30 provides the difference  $\Delta Z$  of the absolute values of  $Z_{in}$  computed considering the frequency behavior of the grounding system ( $Z_{gr}(f)$ ), or just its grounding resistance at 50 Hz ( $R_{gr}$ ) for tower (b) (normalized with respect to the former impedance); as expected from Figure 19a, negligible effects are observed up to 100 kHz, while differences reaching 0.8 p.u. in the MHz range highlight the importance of the grounding system frequency behavior in transients studies.

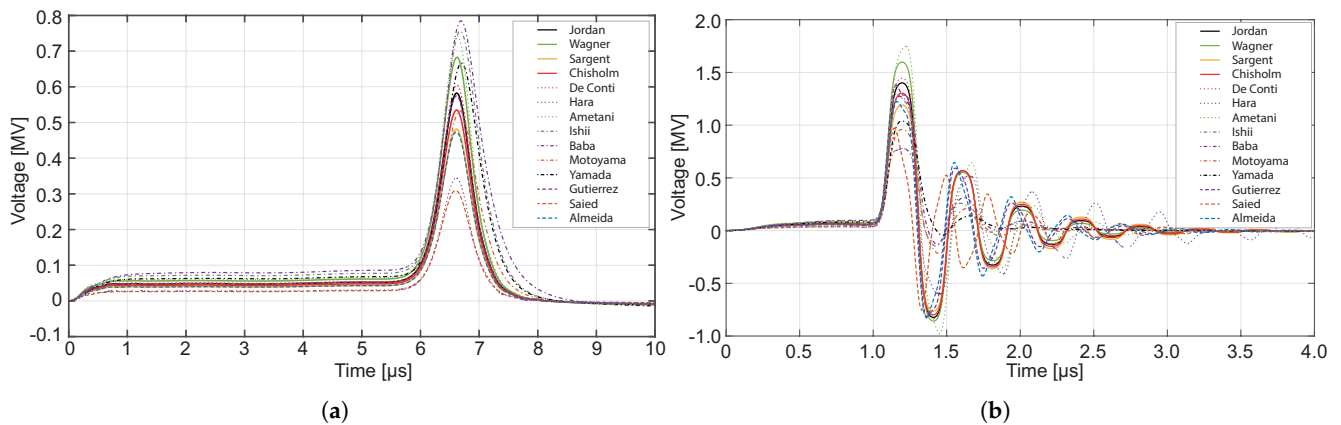


**Figure 22.** Voltage at the top of tower (a) over a PEC plane when the first and subsequent stroke currents in Figure 20 are injected. (a) Response to the first stroke current. (b) Response to the subsequent stroke current.

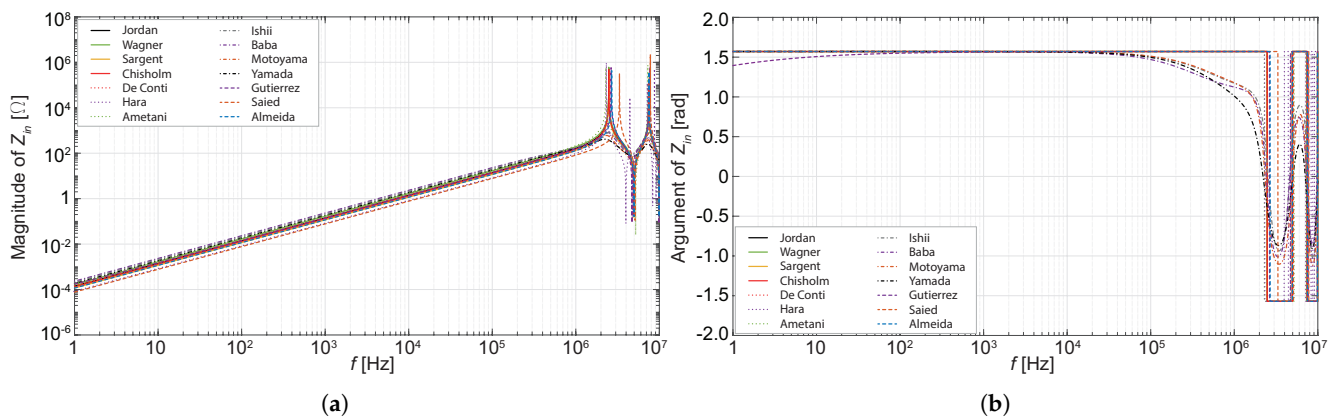


**Figure 23.** Input impedance  $Z_{in}(f)$  seen at the top of tower (a) in Figure 16 over a PEC plane. (a) Magnitude of  $Z_{in}(f)$ . (b) Argument of  $Z_{in}(f)$ .

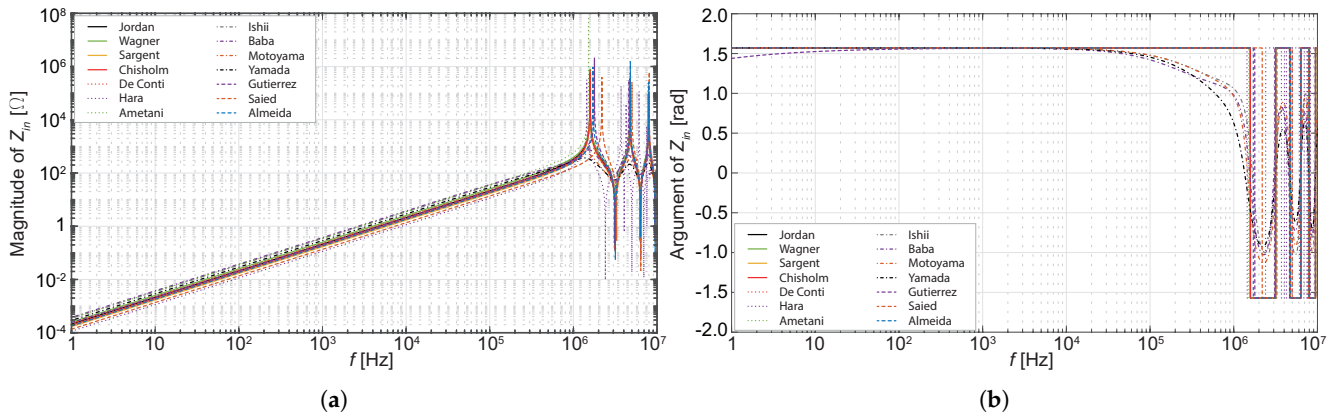


**Figure 24.** Input impedance  $Z_{in}(f)$  seen at the top of tower (b) in Figure 16 over a PEC plane. (a) Magnitude of  $Z_{in}(f)$ . (b) Argument of  $Z_{in}(f)$ .

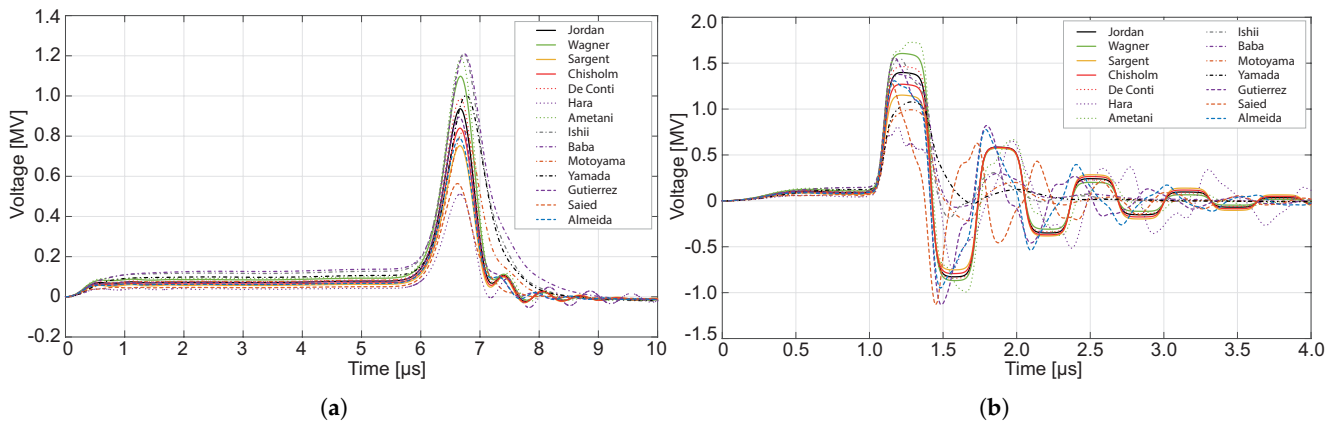


**Figure 25.** Voltage at the top of tower (b) over a PEC plane when the first and subsequent stroke currents in Figure 20 are injected. (a) Response to the first stroke current. (b) Response to the subsequent stroke current.

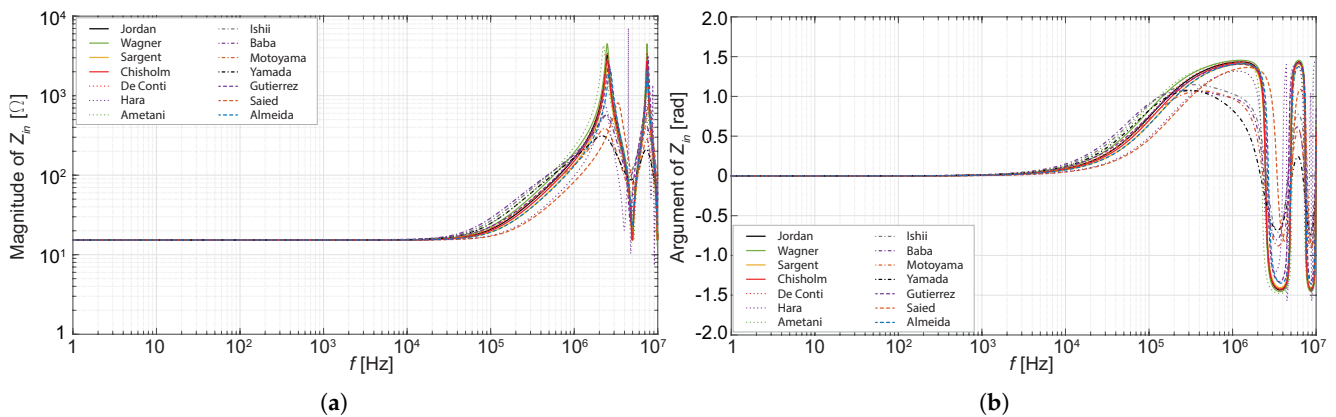


**Figure 26.** Input impedance  $Z_{in}(f)$  seen at the top of tower (a) in Figure 16 over the soil with  $\rho_g = 150 \Omega\text{m}$ ,  $\epsilon_{rg} = 20$ , and  $R_{gr}$  in Table 7. (a) Magnitude of  $Z_{in}(f)$ . (b) Argument of  $Z_{in}(f)$ .

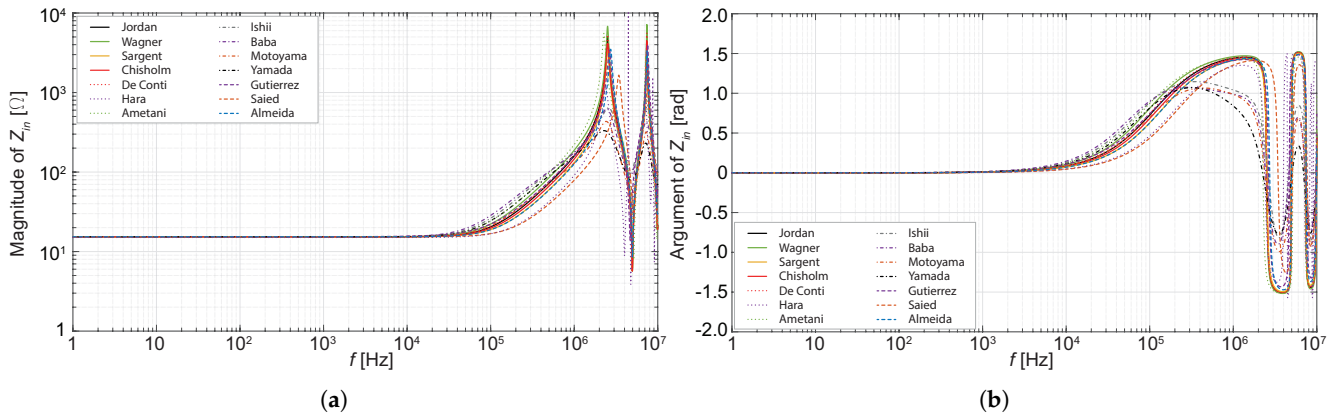


**Figure 27.** Input impedance  $Z_{in}(f)$  seen at the top of tower (a) in Figure 16 over the soil with  $\rho_g = 150 \Omega\text{m}$ ,  $\epsilon_{r_g} = 20$ , and  $Z_{gr}(f)$  in Figure 19. (a) Magnitude of  $Z_{in}(f)$ . (b) Argument of  $Z_{in}(f)$ .

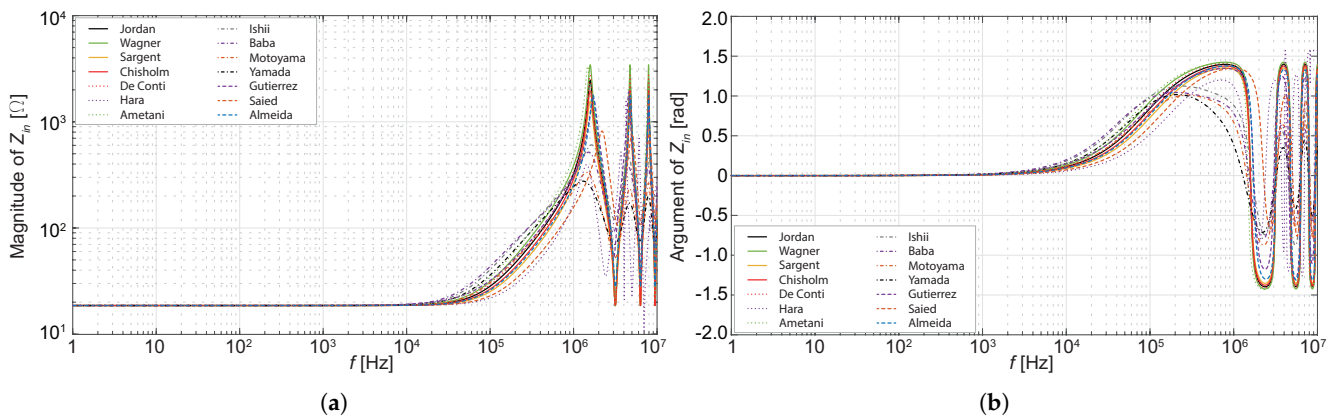


**Figure 28.** Input impedance  $Z_{in}(f)$  seen at the top of tower (b) in Figure 16 over the soil with  $\rho_g = 600 \Omega\text{m}$ ,  $\epsilon_{r_g} = 20$ , and  $R_{gr}$  in Table 7. (a) Magnitude of  $Z_{in}(f)$ . (b) Argument of  $Z_{in}(f)$ .

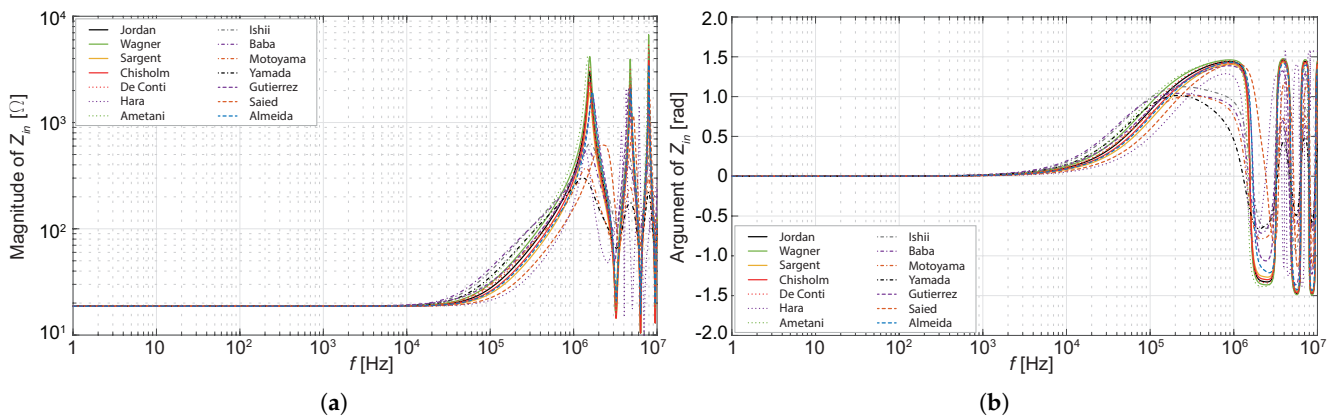


**Figure 29.** Input impedance  $Z_{in}(f)$  seen at the top of tower (b) in Figure 16 over the soil with  $\rho_g = 600 \Omega\text{m}$ ,  $\epsilon_{r_g} = 20$ , and  $Z_{gr}(f)$  in Figure 19. (a) Magnitude of  $Z_{in}(f)$ . (b) Argument of  $Z_{in}(f)$ .

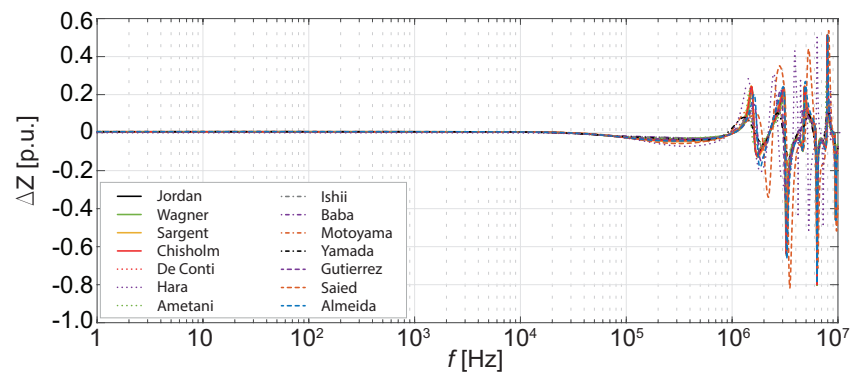


**Figure 30.** Difference  $\Delta Z$  in the absolute values of  $Z_{in}$  computed considering the grounding system modeled by  $Z_{gr}(f)$  or  $R_{gr}$ , normalized to the former  $Z_{in}$  with  $Z_{gr}(f)$  for tower (b) case (soil resistivity  $\rho_g = 600 \Omega\text{m}$ ).

## 6. Conclusions and Final Remarks

This work critically reviewed equivalent circuit models for high-voltage transmission line (TL) towers. Since Jordan proposed the first model in the early 1930s, authors have presented many models to analyze the transient behavior of towers subjected to fast transient waves due to lightning strokes. Despite the availability of complex full-wave models, insulation coordination studies often resort to simple models, which adopt equivalent circuits based on distributed parameters. Indeed, they may be easily implemented into ATP/EMTP-like simulators. Usually, these models derive from magnetostatics or quasi-transverse electromagnetic propagation assumptions that authors claimed to be accurate enough for practical purposes. In this review, tower models have been classified into four main categories: lossless uniform TL models, non-uniform TL models, multiconductor TL models, and multistory models. The review examines the adopted assumptions and their impact on transient studies. Evidence was provided that the available models lead to significant differences in the predicted values of the input impedance seen at the tower top in the frequency domain. Consequently, discrepancies arise in computed voltages in the time domain, affecting insulation studies (which rely on these computations to assess if an apparatus is able to withstand test voltages up to the basic lightning impulse insulation level). Simulations indicated that a crucial parameter in tower modeling is the characteristic impedance of the equivalent TL introduced to represent the tower.

Approaches deriving the tower characteristic impedance from the transient surge impedance in the time domain introduce standard approximations and assumptions. The value of the surge impedance at time  $t = 2h_T/c_T$  is arbitrarily adopted for the constant-valued characteristic impedance  $Z_T$  of the equivalent TL; this hypothesis might be acceptable just for lossless uniform TL models. Indeed, only up to this instant, no effect of reflection from the first discontinuity (namely, the ground interface) will be seen at the tower top, and the line would be represented by  $Z_T$  (real-valued, in the frequency domain). However, no sufficient justification can be provided for the specific choice of the upper limit of the interval  $0 \leq t \leq 2h_T/c_0$ . The most relevant approximation is to define the surge impedance as the ratio of the voltage over the current in the time domain (and *not* through a convolution procedure); in fact, this quantity (along with the derived  $Z_T$ ) would be dependent on the specific adopted current source.

It was demonstrated that the differences ensuing from using different models are significant. In general, models based on approximate parameters tuned on specific tower configurations cannot be adopted in different configurations with an adequate confidence level.

Moreover, it was assessed that the tower model must include an adequate termination accounting for the grounding elements embedded in a dissipative soil: the termination with a perfectly conducting plane yields significant differences concerning the actual system.

Critical points worthy of further investigation are:

- differences between downward and upward waves traveling along the tower;

- possible nonlinearities excited by the corona effect along the tower or by soil ionization;
- frequency-dependent behavior of the grounding grid at the tower base;
- non-TEM nature of the electromagnetic field along the tower.

**Author Contributions:** Formal analysis and software, E.S.; resources, G.P.; supervision, S.C. and R.A. All authors have read and agreed to the published version of the manuscript.

**Funding:** This research received no external funding.

**Informed Consent Statement:** Not applicable.

**Data Availability Statement:** Not applicable.

**Conflicts of Interest:** The authors declare no conflicts of interest.

## References

1. Hileman, A.R. *Insulation Coordination For Power Systems*; CRC Press: Boca Raton, FL, USA, 2018.
2. IEC 60071-2022, TC 99; Insulation Co-Ordination and System Engineering of High Voltage Electrical Power Installations Above 1.0 kV AC and 1.5 kV DC. IEC: Geneva, Switzerland, 2022; pp. 1–901.
3. *IEEE Std C62.82.1-2010 (Revision of IEEE Std 1313.1-1996)*; *IEEE Standard for Insulation Coordination—Definitions, Principles, and Rules*. IEC: Geneva, Switzerland, 2011; pp. 1–22.
4. *IEEE Std 1313.2-1999*; IEEE Guide for the Application of Insulation Coordination. IEEE: New York, NY, USA, 1999; pp. 1–68.
5. Stracqualursi, E.; Araneo, R.; Celozzi, S. The Corona Phenomenon in Overhead Lines: Critical Overview of Most Common and Reliable Available Models. *Energies* **2021**, *14*, 6612. [[CrossRef](#)]
6. Stracqualursi, E.; Araneo, R.; Andreotti, A. The impact of different corona models on FD algorithms for the solution of multiconductor transmission lines equations. *High Voltage* **2021**, *6*, 822–835. [[CrossRef](#)]
7. Stracqualursi, E.; Araneo, R.; Faria, J.B.; Andreotti, A. Protection of distribution overhead power lines against direct lightning strokes by means of underbuilt ground wires. *Electr. Power Syst. Res.* **2022**, *202*, 107571. [[CrossRef](#)]
8. Stracqualursi, E.; Araneo, R.; Faria, J.B.; Andreotti, A. Application of the Transfer Matrix Approach to Direct Lightning Studies of Overhead Power Lines with Underbuilt Shield Wires—Part I: Theory. *IEEE Trans. Power Del.* **2022**, *37*, 1226–1233. [[CrossRef](#)]
9. Stracqualursi, E.; Araneo, R.; Faria, J.B.; Andreotti, A. Application of the Transfer Matrix Approach to Direct Lightning Studies of Overhead Power Lines with Underbuilt Shield Wires—Part II: Simulation Results. *IEEE Trans. Power Del.* **2022**, *37*, 1234–1241. [[CrossRef](#)]
10. Araneo, R.; Andreotti, A.; Brandão Faria, J.; Celozzi, S.; Assante, D.; Verolino, L. Utilization of underbuilt shield wires to improve the lightning performance of overhead distribution lines hit by direct strokes. *IEEE Trans. Power Del.* **2020**, *35*, 1656–1666. [[CrossRef](#)]
11. Andreotti, A.; Araneo, R.; Mahmood, F.; Pierno, A. An accurate approach for the evaluation of the performance of overhead distribution lines due to indirect lightning. *Electr. Power Syst. Res.* **2020**, *186*, 106411. [[CrossRef](#)]
12. Andreotti, A.; Araneo, R.; Mahmood, F.; Piantini, A.; Rubinstein, M. An Analytical Approach to Assess the Influence of Shield Wires in Improving the Lightning Performance due to Indirect Strokes. *IEEE Trans. Power Deliv.* **2020**, *36*, 1491–1498. [[CrossRef](#)]
13. Stracqualursi, E.; Araneo, R. Transient impedance of grounding grids with different soil models. In Proceedings of the 2021 IEEE International Conference on Environment and Electrical Engineering and 2021 IEEE Industrial and Commercial Power Systems Europe (EEEIC/I&CPS Europe), Bari, Italy, 8–11 June 2021; pp. 1–6.
14. Chowdhuri, P.; Li, S.; Yan, P. Rigorous analysis of back-flashover outages caused by direct lightning strokes to overhead power lines. *IEE Proc. Gener. Transm. Distrib.* **2002**, *149*, 58–65. [[CrossRef](#)]
15. Silveira, F.H.; Visacro, S.; De Conti, A.; Mesquita, C.R.d. Backflashovers of Transmission Lines Due to Subsequent Lightning Strokes. *IEEE Trans. Electromagn. Compat.* **2012**, *54*, 316–322. [[CrossRef](#)]
16. Silveira, F.H.; Visacro, S. Lightning performance of transmission lines: Impact of current waveform and front-time on back-flashover occurrence. *IEEE Trans. Power Del.* **2019**, *34*, 2145–2151. [[CrossRef](#)]
17. Silveira, F.H.; Almeida, F.S.; Visacro, S.; Zago, G.M.P. Influence of the current front time representation on the assessment of backflashover occurrence of transmission lines by deterministic and probabilistic calculation approaches. *Electr. Power Syst. Res.* **2021**, *197*, 107299. [[CrossRef](#)]
18. Sindeband, M.; Sporn, P. Lightning and Other Experience with 132-kV. Steel Tower Transmission Lines, and its Bearing on Tower-Line Design from the Continuity of Service Standpoint. *Trans. Am. Inst. Electr. Eng.* **1926**, *45*, 770–790. [[CrossRef](#)]
19. Bewley, L. Critique of Ground Wire Theory. *Trans. Am. Inst. Electr. Eng.* **1931**, *50*, 1–18. [[CrossRef](#)]
20. Fortescue, C.; Fielder, F. Counterpoise tests at Trafford. *Electr. Eng.* **1934**, *53*, 1116–1123. [[CrossRef](#)]
21. Jordan, C.A. Lightning computation for transmission line with overhead ground wires. *Gen. Electr. Rev.* **1934**, *37*, 180–186.
22. Silveira, F.H.; Visacro, S.; Souza, R.E. Lightning performance of transmission lines: Assessing the quality of traditional methodologies to determine backflashover rate of transmission lines taking as reference results provided by an advanced approach. *Electr. Power Syst. Res.* **2017**, *153*, 60–65. [[CrossRef](#)]

23. Almeida, F.S.; Silveira, F.H.; De Conti, A.; Visacro, S. Influence of tower modeling on the assessment of backflashover occurrence on transmission lines due to first negative lightning strokes. *Electr. Power Syst. Res.* **2021**, *197*, 107307. [[CrossRef](#)]
24. Datsios, Z.; Mikropoulos, P. Effect of tower modelling on the minimum backflashover current of overhead transmission lines. In Proceedings of the 19th International Symposium on High Voltage Engineering (ISH), Pilsen, Czech Republic, 23–28 August 2015.
25. Mikropoulos, P.N.; Tsovilis, T.E.; Datsios, Z.G.; Mavrikakis, N.C. Effects of simulation models of overhead transmission line basic components on backflashover surges impinging on GIS substations. In Proceedings of the 45th IEEE International Universities Power Engineering Conference UPEC2010, Cardiff, UK, 31 August–3 September 2010; pp. 1–6.
26. Savic, M.S.; Savic, A.M. Substation Lightning Performance Estimation Due to Strikes Into Connected Overhead Lines. *IEEE Trans. Power Del.* **2015**, *30*, 1752–1760. [[CrossRef](#)]
27. Huang, L.; Zhou, L.; Wu, T.; Hu, C.; Zhang, D.; Wang, D.; Chen, S. A distributed modelling method of the transmission tower and transient response analysis of lightning wave process. *IET Gener. Transm. Distrib.* **2021**, *15*, 3017–3031. [[CrossRef](#)]
28. Grcev, L.; Rachidi, F. On tower impedances for transient analysis. *IEEE Trans. Power Del.* **2004**, *19*, 1238–1244. [[CrossRef](#)]
29. Salarieh, B.; De Silva, H.M.J.; Gole, A.M.; Ametani, A.; Kordi, B. An Electromagnetic Model for the Calculation of Tower Surge Impedance Based on Thin Wire Approximation. *IEEE Trans. Power Del.* **2021**, *36*, 1173–1182. [[CrossRef](#)]
30. Ametani, A.; Triruttanapiruk, N.; Yamamoto, K.; Baba, Y.; Rachidi, F. Impedance and Admittance Formulas for a Multistair Model of Transmission Towers. *IEEE Trans. Electromagn. Compat.* **2020**, *62*, 2491–2502. [[CrossRef](#)]
31. Yamanaka, A.; Nagaoka, N.; Baba, Y. Circuit model of vertical double-circuit transmission tower and line for lightning surge analysis considering TEM-mode formation. *IEEE Trans. Power Del.* **2020**, *35*, 2471–2480. [[CrossRef](#)]
32. Thang, T.H.; Baba, Y.; Nagaoka, N.; Ametani, A.; Takami, J.; Okabe, S.; Rakov, V.A. A Simplified Model of Corona Discharge on Overhead Wire for FDTD Computations. *IEEE Trans. Electromagn. Compat.* **2012**, *54*, 585–593. [[CrossRef](#)]
33. Saito, M.; Ishii, M.; Miki, M.; Tsuge, K. On the Evaluation of the Voltage Rise on Transmission Line Tower Struck by Lightning Using Electromagnetic and Circuit-Based Analyses. *IEEE Trans. Power Del.* **2021**, *36*, 627–638. [[CrossRef](#)]
34. Cao, J.; Du, Y.; Ding, Y.; Li, B.; Qi, R.; Zhang, Y.; Li, Z. Lightning Surge Analysis of Transmission Line Towers With a Hybrid FDTD-PEEC Method. *IEEE Trans. Power Del.* **2022**, *37*, 1275–1284. [[CrossRef](#)]
35. Salarieh, B.; De Silva, H.J.; Kordi, B. Electromagnetic transient modeling of grounding electrodes buried in frequency dependent soil with variable water content. *Electr. Power Syst. Res.* **2020**, *189*, 106595. [[CrossRef](#)]
36. Silva, B.P.; Visacro, S.; Silveira, F.H. HEM-TD: New Time-Domain Electromagnetic Model for Calculating the Lightning Response of Electric Systems and Their Components. *IEEE Trans. Power Deliv.* **2022**, 1–9. [[CrossRef](#)]
37. Salarieh, B.; Kordi, B. Full-wave black-box transmission line tower model for the assessment of lightning backflashover. *Electr. Power Syst. Res.* **2021**, *199*, 107399. [[CrossRef](#)]
38. Zhang, Y.; Li, L.; Han, Y.; Ruan, Y.; Yang, J.; Cai, H.; Liu, G.; Zhang, Y.; Jia, L.; Ma, Y. Flashover Performance Test with Lightning Impulse and Simulation Analysis of Different Insulators in a 110 kV Double-Circuit Transmission Tower. *Energies* **2018**, *11*, 659. [[CrossRef](#)]
39. De Conti, A.; Visacro, S.; Soares, A.; Schroeder, M.A.O. Revision, extension, and validation of Jordan’s formula to calculate the surge impedance of vertical conductors. *IEEE Trans. Electromagn. Compat.* **2006**, *48*, 530–536. [[CrossRef](#)]
40. Slyunyaev, N.N.; Mareev, E.A.; Rakov, V.A.; Golitsyn, G.S. Statistical Distributions of Lightning Peak Currents: Why Do They Appear to Be Lognormal? *J. Geophys. Res. Atmos.* **2018**, *123*, 5070–5089. [[CrossRef](#)]
41. Takahashi, H. Confirmation of the Error of Jordan’s Formula on Tower Surge Impedance. *IEEE Trans. Power Energy* **1994**, *114*, 112–113. [[CrossRef](#)]
42. Wagner, C.F.; Hileman, A.R. A New Approach to the Calculation or the Lightning Performance of Transmission Lines III—A Simplified Method: Stroke to Tower. *AIEE Trans. Power Appar. Syst.* **1960**, *79*, 589–603. [[CrossRef](#)]
43. Sargent, M.A.; Darveniza, M. Tower Surge Impedance. *IEEE Trans. Power Appl. Syst.* **1969**, *PAS-88*, 680–687.
44. Chisholm, W.A.; Chow, Y.L.; Srivastava, K.D. Surge response of transmission towers. *Can. Electr. Eng. J.* **1982**, *7*, 34–36. [[CrossRef](#)]
45. Chisholm, W.A.; Chow, Y.L.; Srivastava, K.D. Travel Time of Transmission Towers. *IEEE Trans. Power Appl. Syst.* **1985**, *PAS-104*, 2922–2928.
46. Rondon, D.; Vargas, M.; Herrera, J.; Montana, J.; Torres, H.; Camargo, M.; Jimenez, D.; Delgadillo, A. Influence of grounding system modeling on transient analysis of transmission lines due to direct lightning strike. In Proceedings of the 2005 IEEE Russia Power Tech, St. Petersburg, Russia, 27–30 June 2005; pp. 1–6.
47. Saied, M.M.; Alfuhaid, A.S.; El-Shandwily, M.E. s-domain analysis of electromagnetic transients on nonuniform lines. *IEEE Trans. Power Del.* **1990**, *5*, 2072–2083. [[CrossRef](#)]
48. Oufi, E.; Alfuhaid, A.; Saied, M. Transient analysis of lossless single-phase nonuniform transmission lines. *IEEE Trans. Power Del.* **1994**, *9*, 1694–1700. [[CrossRef](#)]
49. Almeida, M.; De Barros, M.C. Tower modelling for lightning surge analysis using Electro-Magnetic Transients Program. *IEE Proc.-Gener. Transm. Distrib.* **1994**, *141*, 637–639. [[CrossRef](#)]
50. Barros, M.T.C.D.; Almeida, M.E. Computation of electromagnetic transients on nonuniform transmission lines. *IEEE Trans. Power Del.* **1996**, *11*, 1082–1091. [[CrossRef](#)]
51. Hara, T.; Yamamoto, O.; Hayashi, M.; Uenosono, C. Empirical formulas for surge impedance for single and multiple vertical conductors. *IEEE Trans. Power Energy* **1990**, *B-110*, 129–136.

52. Ametani, A.; Kasai, Y.; Sawada, J.; Mochizuki, A.; Yamada, T. Frequency-dependent impedance of vertical conductors and a multiconductor tower model. *IEE Proc. Gener. Transm. Distrib.* **1994**, *141*, 339–345. [[CrossRef](#)]
53. Moreno, P.; Naredo, J.L.; Bermúdez, J.L.; Paolone, M.; Nucci, C.A.; Rachidi, F. Nonuniform transmission tower model for lightning transient studies. *IEEE Trans. Power Del.* **2004**, *19*, 490–496.
54. Gutierrez, J.; Moreno, P.; Guardado, L.; Naredo, J. Comparison of transmission tower models for evaluating lightning performance. In Proceedings of the 2003 IEEE Bologna Power Tech Conference, Bologna, Italy, 23–26 June 2003; Volume 4, 6p.
55. Ishii, M.; Kawamura, T.; Kouno, T.; Ohsaki, E.; Shiokawa, K.; Murotani, K.; Higuchi, T. Multistory transmission tower model for lightning surge analysis. *IEEE Trans. Power Del.* **1991**, *6*, 1327–1335. [[CrossRef](#)]
56. Baba, Y.; Ishii, M. Tower models for fast-front lightning currents. *IEEE Trans. Power Energy* **2000**, *120*, 18–23. [[CrossRef](#)]
57. Hashimoto, S.; Baba, Y.; Nagaoka, N.; Ametani, A.; Itamoto, N. An equivalent circuit of a transmission-line tower struck by lightning. In Proceedings of the 2010 30th IEEE International Conference on Lightning Protection (ICLP), Cagliari, Italy, 13–17 September 2010; pp. 1–6.
58. Motoyama, H.; Shinjo, K.; Matsumoto, Y.; Itamoto, N. Observation and analysis of multiphase back flashover on the Okushishiku test transmission line caused by winter lightning. *IEEE Trans. Power Del.* **1998**, *13*, 1391–1398. [[CrossRef](#)]
59. Yamada, T.; Mochizuki, A.; Sawada, J.; Zaima, E.; Kawamura, T.; Ametani, A.; Ishii, M.; Kato, S. Experimental evaluation of a UHV tower model for lightning surge analysis. *IEEE Trans. Power Del.* **1995**, *10*, 393–402. [[CrossRef](#)]
60. Noda, T. A tower model for lightning overvoltage studies based on the result of an FDTD simulation. *IEEE Trans. Power Energy* **2007**, *127*, 379–388. [[CrossRef](#)]
61. Gatta, F.M.; Geri, A.; Lauria, S.; Maccioni, M. Generalized pi-circuit tower grounding model for direct lightning response simulation. *Electr. Power Syst. Res.* **2014**, *116*, 330–337. [[CrossRef](#)]
62. Alemi, M.R.; Sheshyekani, K. Wide-Band Modeling of Tower-Footing Grounding Systems for the Evaluation of Lightning Performance of Transmission Lines. *IEEE Trans. Electromagn. Compat.* **2015**, *57*, 1627–1636. [[CrossRef](#)]
63. Schroeder, M.A.O.; de Barros, M.T.C.; Lima, A.C.S.; Afonso, M.M.; Moura, R.A.R. Evaluation of the impact of different frequency dependent soil models on lightning overvoltages. *Electr. Power Syst. Res.* **2018**, *159*, 40–49. [[CrossRef](#)]
64. Visacro, S.; Silveira, F.H. The Impact of the Frequency Dependence of Soil Parameters on the Lightning Performance of Transmission Lines. *IEEE Trans. Electromagn. Compat.* **2015**, *57*, 434–441. [[CrossRef](#)]
65. Feng, Z.; Wen, X.; Tong, X.; Lu, H.; Lan, L.; Xing, P. Impulse Characteristics of Tower Grounding Devices Considering Soil Ionization by the Time-Domain Difference Method. *IEEE Trans. Power Del.* **2015**, *30*, 1906–1913. [[CrossRef](#)]
66. Lings, R. *EPRI AC Transmission Line Reference Book: 200 kV and Above*, 3rd ed.; Electric Power Research Institute: Palo Alto, CA, USA, 2005.
67. LaForest, J.J. *Transmission Line Reference Book: 345 kV and Above*; Electric Utility Systems Engineering Department: Schenectady, NY, USA, 1981.
68. Menemenlis, C.; Chun, Z.T. Wave Propagation on Nonuniform Lines. *IEEE Trans. Power Appl. Syst.* **1982**, *PAS-101*, 833–839.
69. *CIGRE TB 549; Lightning Parameters for Engineering Applications*. CIGRE: Paris, France, 2013; 118p.
70. Javor, V.; Lundengård, K.M.; Rančić, M.P.; Silvestrov, S. Analytical representation of measured lightning currents and its application to electromagnetic field estimation. *IEEE Trans. Electromagn. Compat.* **2017**, *60*, 1415–1426. [[CrossRef](#)]
71. Uman, M.A.; Krider, E.P. A review of natural lightning: Experimental data and modeling. *IEEE Trans. Electromagn. Compat.* **1982**, *EMC-24*, 79–112.
72. Kawai, M. Studies of the surge response on a transmission line tower. *IEEE Trans. Power Appl. Syst.* **1964**, *83*, 30–34. [[CrossRef](#)]
73. Breuer, G.; Schultz, A.; Schломann, R.; Price, W. Field studies of the surge response of a 345-kV transmission tower and ground wire. *Trans. Am. Inst. Electr. Eng. Part III Power Appar. Syst.* **1958**, *76*, 1392–1396. [[CrossRef](#)]
74. Motoyama, H.; Matsubara, H. Analytical and experimental study on surge response of transmission tower. *IEEE Trans. Power Del.* **2000**, *15*, 812–819. [[CrossRef](#)]
75. Chisholm, W.A.; Chow, Y.; Srivastava, K.D. Lightning Surge Response Of Transmission Towers. *IEEE Trans. Power Appl. Syst.* **1983**, *PAS-102*, 3232–3242.
76. Motoyama, H.; Kinoshita, Y.; Nonaka, K. Experimental study on lightning surge response of 500-kV transmission tower with overhead lines. *IEEE Trans. Power Del.* **2008**, *23*, 2488–2495. [[CrossRef](#)]
77. Velasco, J.A.M. *Power System Transients: Parameter Determination*; CRC Press: Boca Raton, FL, USA, 2010.
78. Lundholm, R.; Finn, R.B.; Price, W.S. Calculation of Transmission Line Lightning Voltages by Field Concepts. *Trans. Am. Inst. Electr. Eng. Part III Power Appar. Syst.* **1957**, *76*, 1271–1281. [[CrossRef](#)]
79. Anderson, J.G.; Hagenguth, J.H. Magnetic Fields Around a Transmission Line Tower. *Trans. Am. Inst. Electr. Eng. Part III Power Appar. Syst.* **1958**, *77*, 1644–1649. [[CrossRef](#)]
80. Rothwell, E.J.; Cloud, M.J. *Electromagnetics*; CRC Press: Boca Raton, FL, USA, 2018.
81. Whitehead, J.T.; Chisholm, W.A.; Anderson, J.; Clayton, R.; Elahi, H.; Eriksson, A.; Grzybowski, S.; Hileman, A.; Janischewskyj, W.; Longo, V.; et al. Estimating lightning performance of transmission line 2—Updates to analytical models. *IEEE Trans. Power Del.* **1993**, *8*, 1254–1267.
82. Baba, Y.; Rakov, V.A. On the interpretation of ground reflections observed in small-scale experiments simulating lightning strikes to towers. *IEEE Trans. Electromagn. Compat.* **2005**, *47*, 533–542. [[CrossRef](#)]

83. Bermudez, J.L.; Gutierrez, J.; Chisholm, W.; Rachidi, F.; Paolone, M.; Moreno, P. A reduced-scale model to evaluate the response of tall towers hit by lightning. In Proceedings of the SICEL'2001, Bogotá, Colombia, 2001.
84. Hara, T.; Yamamoto, O. Modelling of a transmission tower for lightning-surge analysis. *IEE Proc. Gener. Transm. Distrib.* **1996**, *143*, 283–289. [[CrossRef](#)]
85. Deri, A.; Tevan, G.; Semlyen, A.; Castanheira, A. The Complex Ground Return Plane a Simplified Model for Homogeneous and Multi-Layer Earth Return. *IEEE Trans. Power Appl. Syst.* **1981**, *100*, 3686–3693. [[CrossRef](#)]
86. Ueda, T.; Ito, T.; Watanabe, H.; Funabashi, T.; Ametani, A. A comparison between two tower models for lightning surge analysis of 77 kV system. In Proceedings of the PowerCon 2000, 2000 IEEE International Conference on Power System Technology. Proceedings (Cat. No. 00EX409), Perth, WA, Australia, 4–7 December 2000; Volume 1, pp. 433–437.
87. Ishii, M.; Baba, Y. Numerical electromagnetic field analysis of tower surge response. *IEEE Trans. Power Del.* **1997**, *12*, 483–488. [[CrossRef](#)]
88. Baha, Y.; Ishii, M. Numerical electromagnetic field analysis on lightning surge response of tower with shield wire. *IEEE Trans. Power Del.* **2000**, *15*, 1010–1015. [[CrossRef](#)]
89. Baba, Y.; Ishii, M. Numerical electromagnetic field analysis on measuring methods of tower surge impedance. *IEEE Trans. Power Del.* **1999**, *14*, 630–635. [[CrossRef](#)]
90. Motoyama, H.; Kinoshita, Y.; Nonaka, K.; Baba, Y. Experimental and Analytical Studies on Lightning Surge Response of 500-kV Transmission Tower. *IEEE Trans. Power Del.* **2009**, *24*, 2232–2239. [[CrossRef](#)]
91. Paul, C.R. *Analysis of Multiconductor Transmission Lines*; John Wiley and Sons: Hoboken, NJ, USA, 2008.
92. Guo, X.; Fu, Y.; Yu, J.; Xu, Z. A non-uniform transmission line model of the  $\pm 1100$  kV UHV tower. *Energies* **2019**, *12*, 445. [[CrossRef](#)]
93. Yamanaka, A. Lightning Surge Analysis of Transmission Lines Using Circuit Models Considering Electromagnetic Phenomena. Ph.D. Thesis, Doshisha University, Kyoto, Japan, 2021.
94. Yamanaka, A.; Nagaoka, N.; Baba, Y. Circuit Model of an Overhead Transmission Line Considering the TEM-Mode Formation Delay. *IEEJ Trans. Electr. Electron. Eng.* **2021**, *16*, 888–895. [[CrossRef](#)]
95. Gatta, F.M.; Geri, A.; Lauria, S.; Maccioni, M.; Palone, F. Lightning Performance Evaluation of Italian 150 kV Sub-Transmission Lines. *Energies* **2020**, *13*, 2142. [[CrossRef](#)]
96. Datsios, Z.G.; Stracqualursi, E.; Araneo, R.; Mikropoulos, P.N.; Tsovilis, T.E. Estimation of the Minimum Backflashover Current and Backflashover Rate of a 150 kV Overhead Transmission Line: Frequency and Current-Dependent Effects of Grounding Systems. In Proceedings of the 2022 IEEE International Conference on Environment and Electrical Engineering and 2022 IEEE Industrial and Commercial Power Systems Europe (EEEIC/I&CPS Europe), Prague, Czech Republic, 2022, *submitted*.
97. Conti, A.D.; Visacro, S. Analytical Representation of Single- and Double-Peaked Lightning Current Waveforms. *IEEE Trans. Electromagn. Compat.* **2007**, *49*, 448–451. [[CrossRef](#)]
98. Gameraota, W.R.; Elismé, J.O.; Uman, M.A.; Rakov, V.A. Current Waveforms for Lightning Simulation. *IEEE Trans. Electromagn. Compat.* **2012**, *54*, 880–888. [[CrossRef](#)]